AD-A137 549 PLASMA CURRENT AND CONDUCTIVITY EFFECTS ON HOSE INSTABILITY(U) NAVAL RESEARCH LAB WASHINGTON DC M LAMPE ET AL. 26 JAN 84 NRL-MR-5140 1/1

UNCLASSIFIED F/G 20/8 NL

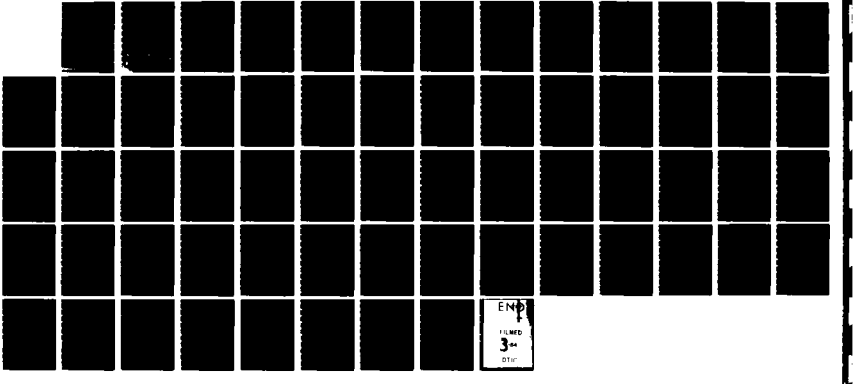

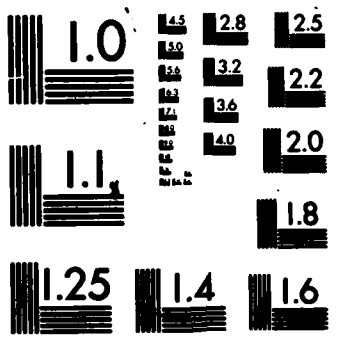

MICROCOPY RESOLUTION TEST CHART
NATIONAL BUREAU OF STANDARDS-1963-A

(2)

NRL Memorandum Report 5140

Plasma Current and Conductivity Effects on Hose Instability

M. LAMPE, W. SHARP,* AND R. HUBBARD**

Plasma Theory Branch
Plasma Physics Division

**Science Applications, Inc.*
McLean, VA 22102

***JAYCOR, Inc.*
Alexandria, VA 22304

AD A137549

January 26, 1984

This work was supported by the Defense Advanced Research Projects Agency under ARPA Order 4395, Amendment No. 9, monitored by the Naval Surface Weapons Center under N60921-83-WR-W0088.

DTIC ELECTE FEB 06 1984 E

NAVAL RESEARCH LABORATORY
Washington, D.C.

Approved for public release; distribution unlimited.

84 02 6 052

SECURITY CLASSIFICATION OF THIS PAGE (When Data Entered)

REPORT DOCUMENTATION PAGE	READ INSTRUCTIONS BEFORE COMPLETING FORM
1. REPORT NUMBER: NRL Memorandum Report 5140 — 2. GOVT ACCESSION NO.: AD-A139 540	3. RECIPIENT'S CATALOG NUMBER:
4. TITLE (and Subtitle): PLASMA CURRENT AND CONDUCTIVITY EFFECTS ON HOSE INSTABILITY	5. TYPE OF REPORT & PERIOD COVERED: Interim report on a continuing NRL problem.
	6. PERFORMING ORG. REPORT NUMBER:
7. AUTHOR(s): M. Lampe, W. Sharp,* and R. Hubbard**	8. CONTRACT OR GRANT NUMBER(s):
9. PERFORMING ORGANIZATION NAME AND ADDRESS: Naval Research Laboratory, Washington, DC 20375	10. PROGRAM ELEMENT, PROJECT, TASK AREA & WORK UNIT NUMBERS: 47-0900-0-3
11. CONTROLLING OFFICE NAME AND ADDRESS: Defense Advanced Research Projects Agency, Arlington, VA 22209	12. REPORT DATE: January 26, 1984
	13. NUMBER OF PAGES: 61
14. MONITORING AGENCY NAME & ADDRESS(if different from Controlling Office)	15. SECURITY CLASS. (of this report): UNCLASSIFIED
	15a. DECLASSIFICATION/DOWNGRADING SCHEDULE:

16. DISTRIBUTION STATEMENT (of this Report)

Approved for public release; distribution unlimited.

17. DISTRIBUTION STATEMENT (of the abstract entered in Block 20, if different from Report)

18. SUPPLEMENTARY NOTES

*Present address: Science Applications, Inc., McLean, VA 22102
**Present address: JAYCOR, Inc., Alexandria, VA 22304

(Continues)

19. KEY WORDS (Continue on reverse side if necessary and identify by block number)

Charged particle beam
Electron beam
Intense relativistic electron beam
Beam propagation
Hose instability
Resistive instabilities

20. ABSTRACT (Continue on reverse side if necessary and identify by block number)

Hose instability dispersion relations are derived for a relativistic beam propagating in weakly ionized gas, which include a self-consistent treatment of the spatial and temporal evolution of plasma conductivity and plasma current. In some regimes the results are dramatically different from these found previously for a beam propagating in a fixed conductivity channel. For example, the hose growth rate is found to decrease with increasing beam I_b for a beam propagating in initially neutral

(Continues)

DD FORM 1 JAN 73 1473 EDITION OF 1 NOV 65 IS OBSOLETE
S/N 0102-014-6601

SECURITY CLASSIFICATION OF THIS PAGE (When Data Entered)

18. SUPPLEMENTARY NOTES (Continued)

This work was supported by the Defense Advanced Research Projects Agency under ARPA Order 4395, Amendment No. 9, monitored by the Naval Surface Weapons Center under N60921-83-WR-W0088.

20. ABSTRACT (Continued)

gas, even though the plasma return current fraction increases rapidly with I_b. As another example, it is found that an externally driven discharge current can completely eliminate hose instability in a fixed conductivity channel, but causes only a weak decrease in growth rate when the plasma conductivity is modeled self-consistently.

CONTENTS

I. Introduction 1

II. Instability of the Beam Body 6

A. Assumptions and Formalism 6

B. Calculation of the Perturbed Beam Current 12

1. Spread Mass Model 13

2. Multi Component Model 15

3. Vlasov Calculation of $\hat{J}_b$ (r) 17

C. Dispersion Relations 18

III. Instability of the Beam Tail 27

IV. Multi-Component Simulations 33

A. VIPER Model Description 33

B. VIPER Simulation of a 10 kA Beam 35

V. Conclusions 39

Acknowledgments 39

Appendix 40

References 56

Accession For	
NTIS GRA&I	☒
DTIC TAB	☐
Unannounced	☐
Justification	
By	
Distribution/	
Availability Codes	
Dist	Avail and/or Special
A-1	

PLASMA CURRENT AND CONDUCTIVITY EFFECTS ON HOSE INSTABILITY

1. Introduction

Several recent papers have developed linear theories of the hose instability of a pinched charged particle beam, propagating in a resistive plasma channel within a neutral gas.[1-5] In the published analytic work to date, elaborate models have been developed to treat the beam dynamics, but the plasma has been represented simply as a fixed ohmic conductivity channel $\sigma(r)$, independent of time and axial position z. For the case of a beam propagating into initially neutral or weakly ionized gas the channel conductivity is formed by beam ionization of the gas, and therefore should be treated self-consistently with the beam dynamics. The significance of this linkage has been understood for some time, and two specific effects have been pointed out by Briggs, Lee, and co-workers[6] for the case of beam propagation into neutral gas. First, the equilibrium conductivity $\sigma_o(r,\zeta)$ increases monotonically with distance $\zeta \equiv v_z t - z$ behind the beam head, in the forward part of the beam where recombination and/or plasma cooling have not yet established a balance with beam-driven ionization and heating. It is thus incorrect there to treat ζ as an ignorable coordinate and Fourier analyze the mode dependence on ζ. Since the growth rate of any resistive instability is largest where σ_o is small, the effects due to increasing σ_o are important. The second effect is seen when there is an appreciable equilibrium plasma return current I_p. If I_p flows in a fixed conductivity channel, an absolute instability results from the magnetic repulsion between I_p and the current I_b of a transversely displaced beam. However if the conductivity channel is formed by the beam itself, the head of the beam cannot be displaced from the channel, which converts the instability into a convective one (provided the effect of phase-mix damping among particles of different betatron frequency is modeled correctly[1,3]). Furthermore, the

Manuscript approved October 11, 1983.

channel, and thus I_p as well, tend to follow the hose distortion of the beam, thereby further reducing the destabilizing effect of spatial separation between I_p and I_b. The consequences of these effects have been worked out, in the low frequency limit and elsewhere in terms of certain parametric representations, by the Livermore group.[6] However hose instability theory has never been treated in the straightforward form of a dispersion relation analysis, valid for all frequencies, that includes self-consistent treatment of the channel conductivity and the plasma current.

In the present paper we include beam-impact ionization and plasma recombination, treated self-consistently, in our conductivity model. These are usually the dominant processes for the case of a weakly ionized gas, except for a short region near the "pinch point" at the front of the beam, where an inductive E_z spike can cause strong avalanche breakdown.[7,8] We further simplify the conductivity model by assuming the electron mobility is constant, i.e., independent of variations in plasma electron temperature. The conductivity then depends only on the electron density. Although this is a reasonably accurate approximation in many cases, we have recently discovered that a number of interesting beam propagation effects can be associated with the temperature dependence. These will be discussed in a future publication.

We also specialize to the limits of an idealized "beam body", discussed in Sec. II, where $I_b(\zeta)$ has reached a plateau, avalanche is assumed to be unimportant, and the plasma electron density n_e is not yet large enough for recombination to be important, and a "beam tail", discussed in Sec. III, where ionization and recombination have reached a balance for the beam equilibrium (but not necessarily for the perturbation). We then show that the inclusion of self-consistent

conductivity physics modifies the problem in a way that is mathematically simple but dramatically changes the physical results. Given any beam dynamics model, and the mathematical machinery to solve for a dispersion relation in the fixed channel case, there is no further difficulty in solving for a complete dispersion relation with a self-consistent treatment of the channel. In fact, a dispersion relation is found in closed form when the relatively simple "spread-mass" model[1,4] of beam dynamics is used.

For relativistic electron beams, it is convenient to use z and ζ as independent variables, rather than z and t. In the beam body, normal modes are found with ζ and z dependence

$$\exp[-i\bar{\omega}\ell n(\zeta/\zeta_o)-i\Omega z/v_z]$$

$$\equiv (\zeta/\zeta_o)^{\bar{\omega}_i}\{\cos[\bar{\omega}_r\ell n(\zeta/\zeta_o)-i\sin[\bar{\omega}_r\ell n(\zeta/\zeta_o)]\}\exp(-i\Omega z/v_z) \tag{1a}$$

rather than the usual form

$$\exp(-i\omega\zeta/v_z - i\Omega z/v_z) \tag{1b}$$

for a fixed channel. In Eq. (1a), ζ_o is an arbitrary index point. In the beam tail, the form (1b) holds, since ζ is an ignorable coordinate in the equilibrium.

Plasma current effects fall into three different regimes. (1) If there is no significant equilibrium plasma current ($|I_p| \ll I_b$), conductivity perturbations play no role. In the tail, $\omega(\Omega)$ is identical to the dispersion relation for a fixed channel. In the body $\bar{\omega}(\Omega)$ is proportional to the frequency $\omega(\Omega)$ that would be found in a fixed channel. In fact, for any

conductivity profile of the form $\sigma_o(r,\zeta) = \sigma_o'(r)\sigma_o''(\zeta)$, the exact ζ dependence of the normal modes is $\exp -i\int_0^\zeta d\zeta' \omega[\Omega;\sigma_o(r,\zeta)]$, where Eq. (1b) with the dispersion relation $\omega=\omega[\Omega;\sigma_o(r)]$ is the normal mode in a fixed channel with conductivity profile $\sigma_o(r)$. (2) If there is a high degree of current neutralization ($0 < I_b + I_p \ll I_b$), I_p is strongly destabilizing but conductivity perturbations, which allow the beam to follow the channel, partially cancel the destabilizing effect. (3) If I_p flows parallel to I_b, as it could for example if an external discharge is applied to the channel, it is possible in a fixed channel to stabilize the hose mode completely, but conductivity perturbations restore the instability by causing the discharge current to follow the unstable beam, rather than guiding it along an established path. In all cases, the perturbed conductivity tends to push the hose growth rate toward the value it would have in the absence of plasma current. In particular, we find that increasing the beam current, thereby increasing both the fractional current neutralization (destabilizing) and the conductivity $\sigma_o(r,\zeta)$ (stabilizing), usually leads overall to a reduced instability growth rate $\bar{\omega}_i$ in the beam body.

The tail of a beam propagating with a large return current in a weakly ionized plasma channel is also subject to another, even more important stabilizing effect: the balance between impact ionization and recombination leads to a channel broader than the beam, so that most of the return current flows outside the beam and has little destabilizing effect. As a result of this and the effects discussed in the previous paragraph, we find that increasing the beam current strongly reduces the growth rate in the tail.

In the present paper, we do not include other sources and sinks in the conductivity model, such as avalanche breakdown, beam heating of the

plasma, or plasma cooling due to radiation, conduction, etc. These effects could be included formally, but would prevent solution for the ζ dependence in the closed forms (1a) or (1b). They are therefore best treated within a numerical scheme that solves for the ζ dependence, e.g. the codes VIPER[9] (multi-component beam dynamics[3]), SIMM1[10] (linearized beam particle simulation), VALIUM[5] (linearized Vlasov solver for beam dynamics), or EMPULSE[11] (spread mass model beam dynamics). In a fully ionized channel, the effects of plasma heating and cooling on hose instability can be expected to be similar to those of ionization and recombination in a weakly ionized channel.

In a previous paper we have discussed the effects of self-consistent conductivity evolution on the sausage mode.[12] The effect there was generally similar but much stronger; channel perturbations, by neutralizing the destabilizing effect of plasma return current, completely stabilized the mode over a wide parameter range.

2. Instability of the Beam Body

A. Assumptions and Formalism

We assume that the beam is highly relativistic ($\gamma \gg 1$), paraxial ($v_\perp \ll v_z$ for all beam particles), and therefore that $v_z \approx c$ for all beam particles. The equilibrium beam profile $J_{bo}(r,\zeta)$ is treated as time-independent. In the beam's body and tail, we assume I_b has reached a constant value. We may also assume that the beam radius $a(\zeta)$, defined by

$$I_b = \pi a^2 J_{bo}(r = 0), \tag{2}$$

and the plasma current I_p are independent of ζ. These latter assumptions are reasonable because resistive decay of the plasma current with ζ occurs slowly, on the monopole decay scale[7,8]

$$c\tau_o(\zeta) = \frac{2\pi\sigma_o(r = 0, \zeta)a^2}{c} \ell n\left(\frac{b}{a}\right), \tag{3}$$

where b is a large radius characterizing the region of space charge neutralization ($b \gg a$), while instability growth is characterized by the much shorter dipole decay ζ scale,[1-3,13]

$$c\tau_1 = \frac{\pi\sigma_o(0,\zeta)a^2}{2c}. \tag{4}$$

Furthermore, the beam body is defined to lie behind the pinch point[7,8], so the conductivity in the body and tail exceeds the value $\sigma = c/4\pi a$ required for space charge neutrality, and with the use of the paraxial approximation Maxwell's equations reduce to Ampere's law for the axial component A of vector potential[1],

$$-\nabla_\perp^2 A = \frac{4\pi}{c} J_z = \frac{4\pi}{c} J_b - \frac{4\pi\sigma}{c} \frac{\partial A}{\partial \zeta}. \tag{5}$$

We define the beam body as the region behind the pinch point, but where recombination (which depends quadratically on n_e) is not yet important. Furthermore, we neglect avalanche ionization in the beam body; this is usually reasonable although avalanche may well be important in the vicinity of the E_z spike at the pinch point, ahead of the body. In a weakly ionized gas, the electron mobility is determined by electron-neutral collisions which depend weakly on temperature; since the dependence of σ on n_e is much more important, we neglect the temperature dependence. In addition, we assume that beam-impact ionization is local, i.e. we neglect any spatial spreading due to high-energy secondary electrons. We may then write a simple equation for the conductivity,

$$\frac{\partial}{\partial \zeta} \sigma(r,\zeta,z) = \kappa J_b(r,\zeta,z), \tag{6}$$

where J_b is the beam current density and κ is here assumed to be a constant for any gas, proportional to the beam-impact ionization frequency and inversely proportional to the plasma electron-neutral collision frequency. In equilibrium, the solution of Eq. (6) is

$$\sigma_o(r,\zeta) = \kappa J_{bo}(r)(\zeta-\zeta_o) + \sigma_o(r,\zeta_o), \tag{7}$$

where ζ_o is the front of the beam body. The first term of Eq. (7) leads to a conductivity profile of the same form as the beam profile. We assume that the second term either is negligible or has the same profile, and absorb it by choosing ζ_o so that

$$\sigma_o(r,\zeta) = \kappa J_{bo}(r)\zeta. \qquad (8)$$

A pre-formed channel narrower or wider than the beam cannot be treated within the simple analytic calculation performed in this section. Qualitatively, a narrower channel decreases the decay lengths (3) and (4) and accentuates the effect of I_p on stability[3], which is stabilizing if $I_p/I_b > 0$ and destabilizing if $I_p/I_b < 0$. The opposite is true for a wider channel.

Since z is an ignorable coordinate of the equilibrium, we may look for normal modes with z-dependence $\exp(-i\Omega z/c)$. We also follow the usual procedure of expanding the azimuthal dependence of A and J_b in a Fourier series $e^{im\theta}$, keeping only the monopole (m = 0) and dipole (m = 1) terms, and linearizing the dipole terms which are treated as small perturbations. All perturbed quantities $\psi(\underset{\sim}{r}_\perp, z, \zeta)$ thus take the form

$$\psi(\underset{\sim}{r}_\perp, z, \zeta) = \psi_1(r,\zeta)\exp(-i\Omega z/c + i\theta).$$

Equation (5) for the dipole A_1 becomes

$$\left(\frac{\partial}{\partial r}\frac{1}{r}\frac{\partial}{\partial r}r - \frac{4\pi\kappa J_{bo}(r)}{c}\zeta\frac{\partial}{\partial\zeta}\right)A_1 = -\frac{4\pi}{c}J_{b1} + \frac{4\pi}{c}\sigma_1\frac{\partial A_o}{\partial\zeta}, \qquad (9)$$

The second term on the right hand side of Eq. (9) represents the current driven in the perturbed channel by the unperturbed electric field $E_{zo} = -\partial A_o/\partial\zeta$. E_{zo} can be expressed in terms of I_p and σ_o,

$$E_{zo}(\zeta) = \frac{J_{po}(r)}{\sigma_o(r,\zeta)}, \qquad (10a)$$

i.e.

$$E_{zo}(\zeta) = \frac{J_{po}(r)}{\kappa J_{bo}(r)\zeta} = \frac{I_p}{\kappa I_b \zeta}, \tag{10b}$$

where we have neglected the weak logarithmic dependence[7,8] of E_{zo} on r, so that $J_{po}(r)$ has the same radial profile as $J_{bo}(r)$ and $\sigma_o(r)$. Using Eq. (10b), Eq. (9) becomes

$$\left(\frac{\partial}{\partial r}\frac{1}{r}\frac{\partial}{\partial r}r - \frac{4\pi\kappa J_{bo}(r)}{c}\zeta\frac{\partial}{\partial\zeta}\right)A_1 = -\frac{4\pi}{c}J_{b1} - \frac{4\pi}{c}\frac{I_p}{\kappa I_b}\frac{\sigma_1}{\zeta}. \tag{11}$$

Next we use the linearized version of Eq. (6), in the form

$$\frac{\partial\sigma_1}{\partial\zeta} \equiv \left(1 + \zeta\frac{\partial}{\partial\zeta}\right)\frac{\sigma_1}{\zeta} = \kappa J_{b1}, \tag{12}$$

to eliminate σ_1 from Eq. (11):

$$\left(1 + \zeta\frac{\partial}{\partial\zeta}\right)\left(\frac{\partial}{\partial r}\frac{1}{r}\frac{\partial}{\partial r}r - \frac{4\pi\kappa J_{bo}(r)}{c}\zeta\frac{\partial}{\partial\zeta}\right)A_1 = -\frac{4\pi}{c}\left(1 + \zeta\frac{\partial}{\partial\zeta} + \frac{I_p}{I_b}\right)J_{b1}. \tag{13}$$

Since Eq. (13) has constant coefficients with respect to the operator $\zeta(\partial/\partial\zeta)$, solutions exist of the form

$$A_1(r,\zeta) = \hat{A}(r)\exp\left[-i\bar{\omega}\ell n(\zeta/\zeta_o)\right]$$

$$= \hat{A}(r)\,\zeta^{\bar{\omega}_i}\left\{\cos\left[\bar{\omega}_r\ell n(\zeta/\zeta_o)\right] - i\sin\left[\bar{\omega}_r\ell n(\zeta/\zeta_o)\right]\right\}. \tag{14}$$

Equation (13) thus reduces to

$$\left(\frac{d}{dr}\frac{1}{r}\frac{d}{dr}r + \frac{4\pi i\bar{\omega}\kappa J_{bo}(r)}{c}\right)\hat{A}(r) = -\frac{4\pi}{c}\left(1 + \frac{I_p/I_b}{1 - i\bar{\omega}}\right)\hat{J}_b(r). \quad (15)$$

When dimensionless variables

$$\bar{r} \equiv r/a, \quad (16)$$

and

$$\bar{J}_{bo}(\bar{r}) = J_{bo}(\bar{r})/J_{bo}(0), \quad (17)$$

are used, Eq. (15) can be rewritten in the form

$$\left(\frac{d}{d\bar{r}}\frac{1}{\bar{r}}\frac{d}{d\bar{r}}\bar{r} + 8i\bar{\omega}\lambda\bar{J}_{bo}(r)\right)\hat{A}(\bar{r}) = -\frac{4\pi}{c}\left(1 + \frac{f}{1 - i\bar{\omega}}\right)\hat{J}_b(\bar{r})a^2, \quad (18)$$

which depends only on the parameters

$$f \equiv I_p/I_b \quad (19)$$

and

$$\lambda \equiv c\frac{d\tau_1}{d\zeta} = \frac{\kappa I_b}{2c}. \quad (20)$$

By way of comparison, Ampere's law takes the form

$$\left[\frac{d}{d\bar{r}}\frac{1}{\bar{r}}\frac{d}{d\bar{r}}\bar{r} + 8i\omega\tau_1\bar{J}_{bo}(r)\right]\hat{A}(\bar{r}) = -\frac{4\pi}{c}\hat{J}_b(\bar{r})a^2 \quad (21)$$

in a fixed channel, where perturbed quantities are of the form

$$A_1(r,\zeta) = \hat{A}(r)e^{-i\omega\zeta/c}. \tag{22}$$

Equations (20) or (21) must be supplemented by an expression for $\hat{J}_b(r)a^2$ as a function of Ω and f and a functional of $\hat{A}(r)$; as we shall see, this calculation is the same for both cases. Thus the hose eigenvalue problem in a self-consistent conductivity channel differs from the problem in a fixed channel in only two ways: first, eigenfunctions are of the form (14) rather than (22), due to the linear increase of the unperturbed conductivity σ_o with ζ in the beam body, and second, there is an extra term on the right hand side of Eq. (18), due to the inclusion of perturbed conductivity. Since several successful methods have been found to treat the problem in a fixed channel, extension of these calculations to Eq. (18) is immediately possible.

B. Calculation of the Perturbed Beam Current

Since all particles have the same axial velocity $v_z \approx c$, the coordinate ζ is a constant of the motion and plays no role in the determination of $\hat{J}_b(r)$, i.e. the form of the ζ dependence, Eq. (14) or (22), and the value of ω or $\bar{\omega}$ do not occur in the particle dynamics. $\hat{J}_b(\bar{r})$ does depend on the time history of the driving potential $\hat{A}(r)e^{-i\Omega z/c}$ (z plays the role of time in the beam frame), and also on equilibrium quantities such as f and the on-axis betatron frequency $\Omega_{\beta o} \equiv [2\pi(1+f)eJ_{bo}(0)/(\gamma mc)]^{1/2}$, where e and m are the electron charge and mass, and γ is the relativistic factor. $\hat{J}_b(\bar{r})$ may be calculated by solving the linearized Vlasov equation[5], by particle simulation[10], or by using either of two simplified beam dynamics models, the multi-component model[3] or the spread mass model[1]. The latter yields a closed-form dispersion relation which is useful for demonstrating general properties, and which the reader can easily solve for any case of interest to him. The other dynamics models are more accurate, but dispersion relations are obtained only through elaborate numerical solutions of the eigenvalue problem. We have developed codes that generate these solutions, and will cite some examples.

1. Spread Mass Model

The spread mass model of E. P. Lee[1,4] is the simplest beam dynamics model that includes the essential feature of phase-mix damping due to betatron frequency spread. According to the spread mass model for the case of a beam with Bennett profile,

$$\bar{J}_{bo}(r) = \frac{\sigma_o(r,\zeta)}{\sigma_o(0,\zeta)} = \frac{1}{(1 + r^2/a^2)^2}, \tag{23}$$

$\hat{J}_b(r,\zeta)$ and $\hat{A}(r,\zeta)$ are represented as rigid sideways displacements of the equilibrium profiles

$$\hat{J}_b(r,\zeta) = - Y(\zeta)(dJ_{bo}/dr) \tag{24a}$$

$$\hat{A}(r,\zeta) = - D(\zeta)(dA_o/dr), \tag{24b}$$

and $Y(\zeta)$ is given as a function of $D(\zeta)$ by[1,14]

$$Y(\zeta) = D(\zeta)[1 + G(\Omega^2/\Omega_{\beta o}{}^2)] \tag{25}$$

where

$$G(x) \equiv 6x\{\tfrac{1}{2} - x + (x-x^2)[\pi i + \ell n(\tfrac{1-x}{x})]\} \text{ for } |x| < 1. \tag{26}$$

The function G(x) is plotted in Fig. 1 for real x. Since the r dependence of all quantities is specified in closed form, Eqs. (15), (23)-(26) immediately reduce to a dispersion relation

$$(1-i\bar{\omega}\lambda)\left(1 + \frac{f}{1-i\bar{\omega}}\right)^{-1} (1+f) = 1 + G\left(\frac{\Omega^2}{\Omega_{\beta o}^2}\right), \tag{27}$$

which yields the solution for $\bar{\omega}(\Omega)$

$$\bar{\omega}\lambda = -\frac{i}{2}\left(\lambda + \frac{f - G(\Omega^2/\Omega_{\beta o}^2)}{1+f}\right) \pm \frac{i}{2}\left[\left(\lambda + \frac{f-G(\Omega^2/\Omega_{\beta o}^2)}{1+f}\right)^2 + 4\lambda G(\Omega^2/\Omega_{\beta o}^2)\right]^{1/2}. \tag{28}$$

We note that for each value of Ω^2 there are two solutions for $\bar{\omega}$, but one of these branches is found to be damped for all real values of Ω, and thus of no interest. Of course Eq. (27) may also be solved numerically for $\Omega(\bar{\omega})$. We may compare Eq. (28) with the well-known dispersion relation for a fixed channel[1,14],

$$\omega\tau_1 = -\frac{i[f-G(\Omega^2/\Omega_{\beta o}^2)]}{1+f}. \tag{29}$$

2. Multi Component Model

The multi-component model of beam dynamics[3] calculates the r dependence of $\hat{J}_b$, rather than assuming a form such as Eq. (24), and it includes radially-localized resonances and other important properties of the exact solution. According to Eqs. (57), (58) and (11) of Ref. 3, the model yields an expression

$$\hat{J}_b(r) = \frac{2r}{1 + f(0)} \int_r^\infty \frac{dR}{R^2} \left(\frac{d}{dR} \frac{1}{R} \frac{d\bar{J}_{bo}(R)}{dR}\right) \left[\frac{\Omega_c^2(R)}{\Omega_{\beta o}^2} - \frac{\omega^2}{\Omega_{\beta o}^2}\right]^{-1} \int_0^R dr' r'^2 \hat{A}(r'), \tag{30}$$

where

$$\Omega_c^2(R) \equiv \frac{4\Omega_{\beta o}^2}{R^2} \int_0^R dr\, r\left(1 - \frac{r^2}{R^2}\right) \bar{J}_{bo}(r) \left[\frac{1 + f(r)}{1 + f(0)}\right], \tag{31a}$$

and, for generality, we have defined

$$f(r) \equiv J_{po}(r)/J_{bo}(r). \tag{31b}$$

Since $J_{bo}(r)$ and $J_{po}(r)$ have the same radial profile in the beam body, $f(r) = f$ and we may rewrite (31a) as

$$\Omega_c^2(R) \equiv \frac{4\Omega_{\beta o}^2}{R^2} \int_0^R dr\, r \left(1 - \frac{r^2}{R^2}\right) \bar{J}_{bo}(r). \tag{31c}$$

Using Eqs. (18), (20) and (30), the eigenvalue problem may be expressed, in analogy with Eq. (61) of Ref. 3, as a fourth-order ordinary differential equation

$$\frac{1}{8} \left(\frac{d}{d\bar{r}} \frac{1}{\bar{r}}\right)^4 \bar{r}^3 \Gamma + i\bar{\omega}\lambda \frac{d}{d\bar{r}} \frac{\bar{J}_{bo}}{\bar{r}^3} \frac{d}{d\bar{r}} \bar{r}^2 \Gamma$$

$$= \left(1 + \frac{f}{1 - i\bar{\omega}}\right)\left(\frac{1}{1 + f}\right) \frac{1}{\bar{r}^2} \frac{d}{d\bar{r}} \frac{1}{\bar{r}} \frac{d\bar{J}_{bo}}{d\bar{r}} \frac{\bar{\omega}_e^2(0)}{\bar{\omega}_e^2(r) - \bar{\omega}^2} \Gamma, \qquad (32)$$

with

$$\Gamma(r) \equiv \frac{1}{r^2} \int_0^r dr' \, r'^2 \, \hat{A}(r') \qquad (33)$$

and boundary conditions

$$\Gamma(0) = \Gamma'(0) = \Gamma'(\infty) = \Gamma''(\infty) = 0. \qquad (34)$$

This differs from the fixed-channel case only through the extra factor $[1 + f(1 - i\bar{\omega})^{-1}]$ on the right hand side of (32). Thus a code which we developed[3] to solve this complicated eigenvalue problem in the fixed-channel case can also be used to find $\bar{\omega}(\Omega)$ in the present case.

3. Vlasov Calculation of $\hat{J}_b(r)$

If the beam equilibrium is taken to be time-independent, and weak scattering of the beam off the gas is neglected, an exact expression for $\hat{J}_b(r)$ in terms of $\hat{A}(r)$ can be obtained by integration of the linearized Vlasov equation along unperturbed beam electron orbits. This procedure yields

$$\hat{J}_b(r) = -e^2 \int d^3p \, \frac{p_z}{p_\perp} \frac{\partial f_{bo}}{\partial p_\perp} \left\{\hat{A}(r) + \frac{\Omega}{c} \int_{-\infty}^{z} dz' \, i\hat{A}(r') \exp\left[i\theta' - i\theta - \frac{i\Omega(z-z')}{c}\right]\right\}, \tag{35}$$

where p is the particle relativistic momentum, p_z and $p_\perp$ are the axial and perpendicular components of p, $f_{bo}(p_z,p_\perp)$ is the beam distribution function, and (r,θ,z) are the particle cylindrical coordinates. $\theta'(z')$ and $r'(z')$ are the unperturbed particle trajectories backward in time, i.e. θ' and r' are the coordinates a particle had when it was at z', if that particle has coordinates θ and r when it is at z. Thus $\theta'(z')$ and $r'(z')$ are also functions of p and of the unperturbed potential A_o.

Equations (35) and either (18) or (21) together constitute a very complicated integral-differential eigenvalue problem. A code, known as VALIUM, has been developed[5] with the capability to solve the fixed-channel case (35) and (21) as well as the self-consistent channel case, Eq. (35) and (18).

C. Dispersion Relations

In this section we discuss the growth spectra $\omega_i(\Omega)$ that result from the dispersion relation derived in closed form in Sec. IIA, or from solution of the eigenvalue problems framed formally in Secs. IIB and IIC. The discussion will be organized in terms of the value of f - either no plasma current (f=0), extensive current neutralization ($0 < 1 + f << 1$), or plasma current flowing parallel to the beam current ($f > 0$), and in terms of the effect of beam-generated perturbations to the conductivity, which is small if $\lambda \lesssim 1$ (low beam current) and large if $\lambda >> 1$ (high beam current). The value of λ depends only on I_b, but the value of f can depend on the properties of the beam head (rise time of I_b and avalanche ionization near the pinch point), and the presence of a pre-formed conductivity channel or an externally imposed E_z field, as well as on I_b. We conclude by surveying the case of beam injection into field-free neutral gas, under conditions where both λ and f depend primarily on the single parameter I_b.

We shall use the spread mass model dispersion relation, Eq. (28), to derive various analytic results in closed form. We also show plots of the dispersion relation for a variety of cases, Figs. 2-5, 7 as calculated from the multi-component model, Eqs. (32)-(34), which is more accurate and which is not immediately accessible to the reader. The numerical values of the key features of the dispersion relations - maximum growth rates and cut-offs - are given in Table 1 for each of these models and for the Vlasov calculation, which is theoretically exact, but subject to numerical uncertainties of perhaps a few percent. We find that both models agree well with the exact result as regards the peak growth rate Max $\bar{\omega}_i$. The multicomponent model also gives an accurate estimate of the width of the

Table 1

Comparison of the key features of the hose dispersion relation in the beam body, as given by the spread mass (SM) model, the multicomponent (MC) model, and a Vlasov (V) calculation. Here Max $\bar{\omega}_i$ is the peak power-law growth exponent for growth in ζ and λ Max $\bar{\omega}_i$ is a natural scaled quantity from the theory, Ω_m is the value of Ω for which $\bar{\omega}_i(\Omega) = \text{Max } \bar{\omega}_i$, Ω_c is the largest value of Ω for which $\bar{\omega}_i(\Omega) > 0$, and $\Omega_{\beta o}$ is the on-axis betatron frequency. These values, for the multicomponent model, can also be read directly from the dispersion relation curves of Figs. 2-5.

λ	f	λ Max $\bar{\omega}_i$			$\Omega_m/\Omega_{\beta o}$			$\Omega_c/\Omega_{\beta o}$		
		SM	MC	V	SM	MC	V	SM	MC	V
0	1.0	-0.17	-0.17		0.52	0.53				
	0.5	0.12	0.11		0.52	0.55		0.62	0.66	
	0	0.69	0.66		0.52	0.61		0.71	0.78	
	-0.25	1.25	1.23		0.52	0.62		0.73	0.82	
	-0.5	2.4	2.4		0.52	0.63		0.76	0.87	
	-0.7	4.6	4.9		0.52	0.67		0.78	0.90	
	-0.9	15.9	18.7		0.52	0.79		0.79	0.96	
0.044	1.0	0.04	0.04		0.38	0.42		0.46	0.46	
	0.5	0.16	0.14		0.51	0.53		0.63	0.67	
	0	0.69	0.66	0.74	0.52	0.61	0.6	0.71	0.78	0.8
	-0.25	1.22	1.21	1.34	0.52	0.62	0.65	0.73	0.82	0.9
	-0.5	2.3	2.4	2.5	0.52	0.63	0.66	0.75	0.87	0.9
	-0.7	4.6	4.8	5.0	0.52	0.67	0.68	0.78	0.90	0.9
	-0.9	15.8	18.7	17.2	0.52	0.79	0.7	0.79	0.96	0.9
0.44	1.0	0.32	0.29		0.51	0.51		0.68	0.72	
	0.5	0.40	0.36	0.42	0.51	0.53	0.51	0.69	0.73	
	0	0.69	0.66	0.74	0.52	0.61	0.6	0.71	0.78	0.8
	-0.25	1.12	1.11	1.21	0.52	0.62	0.61	0.73	0.82	
	-0.5	2.3	2.2	2.5	0.52	0.63	0.62	0.75	0.86	0.9
	-0.7	4.3	4.5	4.7	0.52	0.67	0.63	0.77	0.89	
	-0.9	15.5	18.3	18.9	0.52	0.80	0.71	0.78	0.95	
4.4	1.0	0.64	0.60		0.54	0.62		0.75	0.82	
	0.5	0.65	0.62		0.53	0.62		0.74	0.80	
	0	0.69	0.66	0.74	0.52	0.61	0.6	0.71	0.78	0.8
	-0.25	0.74	0.70	0.82	0.52	0.55	0.56	0.68	0.77	
	-0.5	0.88	0.87	1.11	0.52	0.55	0.58	0.65	0.78	0.9
	-0.7	1.7	2.1	2.3	0.52	0.67	0.65	0.67	0.85	
	-0.9	11.9	14.2	14.8	0.52	0.78	0.72	0.76	0.95	0.9

unstable spectrum and the value Ω_m for peak growth [$\bar{\omega}_i(\Omega_m) = \text{Max } \bar{\omega}_i$], but the spread mass model underestimates both the spectral width and the value of Ω_m.

$I_p = 0$

In the case of no equilibrium plasma current, $I_p = f = 0$, Eq. (18) for $\lambda\bar{\omega}(\Omega)$ in the beam body becomes formally identical to Eq. (21), which determines $\tau_1\omega(\Omega)$ in a fixed conductivity channel. Thus the dispersion relation for power-law growth in the beam body, $\lambda\bar{\omega}(\Omega)$, is identical to the dispersion relation for exponential growth in a fixed channel with $f = 0$. Perturbed conductivity plays no role when $f = 0$, since the absence of equilibrium plasma current indicates that $E_{zo} = 0$ and thus a dipole conductivity σ_1 yields no dipole plasma current $E_{zo}\sigma_1$. When the spread mass model is used, the dispersion relation is given by Eq. (29),

$$\lambda\bar{\omega}(\Omega) = iG\left(\Omega^2/\Omega_{\beta o}{}^2\right), \tag{36}$$

and is shown in Fig. 1. For the spread mass model, the peak growth rate is $\text{Max } \bar{\omega}_i = 0.69\ \lambda^{-1}$ at $\Omega/\Omega_{\beta o} = 0.52$, and the unstable spectrum runs from $\Omega = 0$ to $\Omega = 0.71\ \Omega_{\beta 0}$. The equivalent result from the multicomponent model is shown as the $f = 0$ curve in Fig. 2; the peak growth rate is $\text{Max } \bar{\omega}_i = 0.65\ \lambda^{-1}$ at $\Omega/\Omega_{\beta 0} = 0.61$, and the unstable spectrum runs from $\Omega = 0$ to $\Omega = 0.78\ \Omega_{\beta 0}$. We note that $\bar{\omega}_i(0) = 0$, an exact result.

Low Beam Current ($\lambda \to 0$)

Next we consider the limit $\lambda \to 0$, which corresponds to low beam current, as seen in Eq. (20). For example, in air we use the estimate[15]

$$\lambda = 0.044\ I_b \tag{37}$$

where I_b is in kiloamperes. Equation (37) corresponds to $\epsilon = 8.8 \times 10^{-4}$ cm/statcoul in Eq. (6).

In the limit $\lambda \to 0$, for any given value of f and for any beam dynamics model the dispersion relation for $\lambda\bar{\omega}(\Omega)$ is identical to the dispersion relation for $\tau_1\omega(\Omega)$ in a fixed channel. This is because the conductivity changes slowly in this limit, and thus the effect of conductivity perturbations is negligible. For example, the spread mass dispersion relation, Eq. (28), reduces to[1,14]

$$\lambda\bar{\omega} = -\,i\,\frac{f - G(\Omega^2/\Omega_{3o}{}^2)}{1 + f}\,. \tag{38}$$

If $f < 0$, there is an unstable mode at $\Omega = 0$ with growth rate $\bar{\omega}_i(0) = \lambda^{-1}[-f(1 + f)^{-1}]$, an exact result, but the most unstable mode is still at $\Omega/\Omega_{\beta o} = 0.52$, where $\bar{\omega}_i = \text{Max}\ \bar{\omega}_i = \lambda^{-1}\,(-f + 0.69)(1 + f)^{-1}$. The equivalent result from the multi-component model is shown in Fig. 2 for several values of f. The peak growth rate for any given value of f is close to that given by the spread mass model, as seen in Table 1, but the value of Ω for peak growth increases with the return current fraction, and the unstable spectrum given by the multi-component model is considerably broader. The multi-component dispersion relation is close to the Vlasov result, as seen in Table 1.

If the beam is propagating into initially unionized gas with $\lambda \ll 1$, Eq. (14), together with Eq. (38) or Fig. 2, indicates very rapid power-law growth of the instability. If on the other hand, the gas is pre-ionized or rapidly ionized at the beam head, the limit $\lambda \ll 1$ should

correspond to propagation in a fixed channel. This limit may be obtained by writing

$$\omega = \bar{\omega}c/\zeta_o \tag{39a}$$

and expanding $\ln(\zeta/\zeta_o)$ in Eq. (14) to obtain exponential mode growth at a rate independent of λ,

$$A_1(r,\zeta) = \hat{A}(r)\exp[-i\omega(\zeta - \zeta_o)/c]. \tag{39b}$$

Current Neutralized Case, $f < 0$, Increasing Values of λ

Figures 3-5 show the multicomponent dispersion relation for a sequence of increasing values of λ. We note that for any given value of f in the range $-1 < f < 0$ (partial current neutralization), $\lambda\bar{\omega}_i$ decreases as λ increases. Thus, if f is held fixed, the growth rate $\bar{\omega}_i$ decreases with increasing I_b for two reasons: $\omega \propto \lambda^{-1} \propto I_b^{-1}$ because $\sigma_o(\zeta)$ grows faster for large I_b, and additionally because for large I_b the conductivity channel tends to follow the perturbations of the beam current, thus inhibiting the spatial separation of I_b and I_p. The latter effect is most dramatic at $\Omega = 0$, where

$$\lambda\bar{\omega}_i = \begin{cases} -f(1+f)^{-1} - \lambda, & \text{if } -f(1+f)^{-1} - \lambda > 0 \\ 0, & \text{otherwise.} \end{cases} \tag{40}$$

For moderate values of f and large values of λ, λ Max $\bar{\omega}_i$ is reduced by about 30% by the effect of perturbed conductivity over the range $0 \leq \lambda < 4.4$ covered in Figs. 2-5. In the limit $f \to -1$, however, the

stabilizing effect of perturbed conductivity goes away and $\bar{\omega}_i \propto \lambda^{-1}$ for fixed f.

The spread mass dispersion relation, Eq. (28), differs from the multicomponent results mainly in that the unstable spectrum is narrower and the peak growth rate is always at $\Omega = 0.52\ \Omega_{\beta 0}$ for the former, as seen in Table 1. The Vlasov unstable spectral width is close to the multicomponent results.

I_p Parallel to I_b, f > 0, Increasing Values of λ

The effects of perturbed conductivity are most dramatic if f > 0, i.e. the plasma current flows parallel to the beam current (as may occur in the back half of a triangular beam pulse where I_b is falling, or in the presence of a strong external discharge). Figure 2 shows that when $\lambda \to 0$ the hose mode is damped for all values of Ω if $f \gtrsim 0.7$, but Figs. 3-5 show that even the smallest positive λ leads to a full range of unstable modes, and that if $\lambda >> 1$ the external discharge does not even reduce the growth rate significantly. (See also Table I.) In this limit the plasma current tends to follow the distorted beam, rather than constraining the beam to follow a straight channel. [Of course a discharge may also exert a strong stabilizing effect by providing a pre-existing conductivity at the beam head; mathematically this corresponds to increasing ζ_o in Eq. (7). This effect is not due to the continuing presence of discharge current during transport of the beam.]

Limit of Large λ

In the limit of very large λ and fixed f,

$$\lambda \gg (1 + f)^{-1},$$

Eq. (28) reduces to the dispersion relation

$$\bar{\omega}\lambda = iG(\Omega^2/\Omega_{\beta o}^2), \tag{41}$$

identical to the dispersion relation for $\tau_{1\mu}(\Omega)$ in a fixed channel with $f = 0$. In this limit, the conductivity channel follows the hose distortions of the beam so easily that I_p does not separate from I_b and presence of equilibrium plasma current has no destabilizing effect on hose stability. However our assumption that the plasma is weakly ionized normally will break down before this limit is reached.

Beam Injected into Neutral Gas, No Discharge Current

Of particular interest is the scaling of hose growth with I_b, for the case of beam propagation in an initially neutral gas with no externally driven plasma current. We have seen that the hose dispersion relation depends on two parameters: λ, which is proportional to I_b, and f, which depends in general on the radius a and the rise-time τ_r of $I_b(\zeta)$, as well as on the value of I_b in the beam body. However a simple scaling is possible for the case in which $I_b(\zeta)$ rises quickly to its plateau value ($\tau_r/a \lesssim 20$ to 40), and avalanche ionization due to the E_z-spike at the pinch point is unimportant ($E_z/\rho \lesssim$ 100 keV/cm-atm in air, i.e. gas density not too low and beam current density not too high). Under these conditions, $f(\zeta)$ depends only on I_b; after reaching a maximum at the pinch point, it levels off to a value that varies slowly with ζ and may be estimated as[8]

$$-\frac{f}{1-f} \approx \lambda. \tag{42}$$

To obtain an expression in closed form for the scaling of the peak growth rate with I_b, we use (42) and (37) in the spread mass dispersion relation (28). Noting that the peak growth rate Max $\bar{\omega}_i$ from Eq. (28) always occurs at $\Omega/\Omega_{\beta o} = 0.52$ where G_r reaches its maximum value 0.69, we find that

$$\text{Max } \bar{\omega}_i = \frac{G_r}{-2f} + \frac{1}{2f} \text{ Re } [G^2 - 4Gf(1+f)]^{1/2} \tag{43}$$

with $G_r = 0.69$, $G_i = 1.01$. The quantity in brackets is slowly varying, so that Max $\bar{\omega}_i$ scales essentially as f^{-1}. Max $\bar{\omega}_i$ from Eq. (43) is plotted as a function of I_b in Fig. 6, using the multicomponent model and Eq. (42); the result differs slightly from Eq. (43). We see that Max $\bar{\omega}_i$ is a monotonically decreasing function that approaches a limit

$$\text{Max } \bar{\omega}_i \to 0.69, \text{ as } \left\{ \begin{matrix} f \to -1 \\ \lambda \to \infty \end{matrix} \right\}. \tag{44}$$

Thus higher current beams, with larger return current fractions $|f|$, are seen to be less unstable.

Equation (42) happens to be the condition for marginal stability of the hose mode with $\Omega = 0$. Since (42) is only a rough estimate of f, and f does vary somewhat even within the beam body, specific cases may have an unstable mode at $\Omega = 0$, but the growth rate $\bar{\omega}_i(0)$ then would be quite small compared to Max $\bar{\omega}_i$. Instability in the range $\Omega \ll \Omega_{\beta o}$ is driven primarily by repulsion between I_b and I_p and has been called the "self-hose", but as seen in Figs. 2-5 there is a smooth transition to the much stronger "high-frequency hose", with a peak growth rate in the range $0.6 < \Omega/\Omega_{\beta 0} < 1$.

In cases where avalanche is important near the pinch point, or where the current rise time τ_r is long $|f|$ can be larger than the estimate given

by Eq. (42), leading to a larger hose growth rate. Several cases, calculated with the multicomponent simulation code VIPER (described in the next section), are also shown in Fig. 6. For these cases, the relativistic factor is $\gamma = 100$, the beam current pulse shape is $I_b(\zeta) = I_{bo}\tanh(\zeta/30a_o)$, the gas is air at standard density, I_{bo} is 4, 10, 40 or 100 kA, and the radius of the beam body is $a_o \approx 0.5\ (I_{bo}/10\ \text{kA})$ cm, so that the current density is the same for the four cases. In order to compare with theory, the initial perturbation was started in the beam body at $\zeta = 30a_o$, and recombination, scattering of the beam and ohmic energy loss were turned off. The hose growth rates seen in Fig. 6 do not deviate greatly from the scaling of Eq. (43).

3. Instability of the Beam Tail

As ζ increases and the plasma electron density n_e becomes large, recombination can become competitive with impact ionization, and thus "saturate" the plasma conductivity σ. This effect can be modeled by extending Eq. (6) to the form

$$\frac{\partial}{\partial \zeta} \sigma_o(r,\zeta) = < J_{bo}(r) - \beta_r \sigma_o^2(r). \tag{45}$$

For simplicity, we neglect temperature dependendence in the recombination coefficient as well as the mobility. For a weakly ionized gas where electron-neutral collisions dominate the resistivity, we then have $\beta_r \equiv \beta_r' \rho_g/\rho_o$, where β_r' is a constant for any given gas species, ρ_g is the gas density, and ρ_o is standard atmospheric density; a typical value for air is $\beta_r \approx 7 \times 10^{-15}$ sec/cm.

The solution to Eq. (45) is

$$\sigma_o(r,\zeta) = \sigma_{sat}(r) \tanh (\beta_r \sigma_{sat} \zeta), \tag{46a}$$

where the saturated value is

$$\sigma_{sat}(r) = [< J_{bo}(r)/\beta_r]^{1/2}. \tag{46b}$$

We see from Eqs. (46) that σ_o saturates first on axis, where σ_{sat} is largest; saturation can occur considerably later off axis. Of course, saturation may not occur during the duration of the beam if J_b or ρ_g is too small.

We consider next an idealized beam tail, where σ_o is saturated at

least out to several beam radii a. We assume, as we did in the beam body, that I_b, I_p and a are constant. With these assumptions, ζ is an ignorable coordinate in the beam tail, and hose eigenmodes are of the form (22).

The perturbed conductivity σ_1 is determined from the linearized equation

$$\frac{\partial \sigma_1}{\partial \xi} = \langle J_{b1} - 2\beta_r \sigma_0 \sigma_1, \tag{47}$$

i.e. from (22),

$$\hat{\sigma}(r) = \frac{\langle \hat{J}_b(r)}{2\beta_r \sigma_0(r) - i\omega}. \tag{48}$$

When we use Eqs. (48), (46b) and (10a) in Eq. (5), the linearized Ampere's law can be written as

$$\left(\frac{1}{\bar{s}} \frac{d}{d\bar{r}} \frac{1}{\bar{r}} \frac{d}{d\bar{r}} \bar{r} + \frac{i\omega\pi\sigma_0(r)a^2}{2c^2}\right)\hat{A}$$

$$= -\frac{\pi}{2c}\left\{1 + \frac{1}{2} f(r)\left[1 - \frac{i\pi\omega\sigma_o(r)a^2}{2\lambda \bar{J}_{bo}(r)c}\right]^{-1}\right\} \hat{J}_b, \tag{49}$$

analogous to Eq. (15) in the beam body. The radial profiles of $J_{po}(r)$ and $\sigma_o(r)$ are essentially identical to each other, but are broader than that of $J_{bo}(r)$, so the radial dependence of $f(r) \equiv J_{po}(r)/J_{bo}(r)$ is important.

As in Sec. II, $\hat{J}_b(r)$ for use in Eq. (49) may be expressed in terms of $\hat{A}(r)$ by using the multi-component model, Eqs. (30) and (31a), or the Vlasov orbit integral, Eq. (35). For the multi-component model, the

resulting eigenvalue equation is

$$\frac{1}{\bar{s}}\left(\frac{d}{d\bar{r}}\frac{1}{\bar{r}}\right)^4 \bar{r}^3\Gamma + i\omega\frac{d}{d\bar{r}}\frac{\pi\sigma_o(r)a^2}{2c^2}\frac{1}{\bar{r}^3}\frac{d}{d\bar{r}}\bar{r}^2\Gamma$$

$$=\left(1+\frac{f(r)}{2}\frac{1}{1-\frac{i\omega}{\lambda\bar{J}_{bo}(r)}\frac{\pi\sigma_o(r)a^2}{2c^2}}\right)\left(\frac{1}{1+f(0)}\right)\frac{1}{\bar{r}^2}\frac{d}{d\bar{r}}\frac{1}{\bar{r}}\frac{d\bar{J}_{bo}}{dr}\frac{\Omega_{\beta o}^2}{\Omega_c^2(r)-\bar{s}^2}\Gamma, \tag{50}$$

where $\Gamma(r)$ is the auxiliary function defined in Eq. (33). Equation (50) is analogous to Eq. (32) and is supplemented by Eq. (31a) and the boundary conditions (34). We shall use Eq. (50) for the analysis and numerical examples used in this section.

The Vlasov form of the eigenvalue equation is obtained by using Eq. (35) in Eq. (49). This integro-differential equation may be solved numerically by our code VALIUM.

In regard to the spread mass model we note that the model in the form of Eqs. (23)-(28) can only be used if $J_{bo}(r)$ and $\sigma_o(r)$ both have Bennett profiles of equal width, and thus is not applicable to the present case.[16]

Figure 7 shows the growth spectrum calculated from Eq. (50) for four cases spanning a wide range of parameter space: $\lambda = 0.044$, $f = -0.042$ (solid curve); $\lambda = 0.44$, $f = -0.30$ (dashed curve); $\lambda = 4.4$, $f = -0.81$ (dotted curve); and $\lambda = 0.44$, $f = +1.0$ (dot-dashed curve). We use the notation $f \equiv I_p/I_b$, even though the spatial profiles of $J_p(r)$ and $J_b(r)$ are different. The first three cases represent roughly beams of 1, 10 and 100 kA injected into neutral air, to the accuracy of our simple conductivity

formula (45), with ζ specified by (37) and our return current scaling given by (42); the fourth case represents a 10 kA beam "guided" by a 10 kA net discharge current.

In each case the radial profile of $J_{bo}(r)$ is taken to be a Bennett profile cut off at three Bennett radii, in the form

$$J_{bo}(r) = \left(1 + \frac{r^2}{a_B^2}\right)^{-2} \frac{1}{1 + \exp\left[2(r - 3a_B)/a_B\right]} .$$

For this profile, the Bennett radius a_B is slightly smaller than the scale radius a defined in Eq. (2). A cut-off is necessary because otherwise the slow radial fall-off of the conductivity profile (46b) would cause essentially all of the plasma current to flow outside the beam. This is one of many mathematical complications[3,8] associated with the slow fall-off of the Bennett profile at large radii; the Bennett profile is a proper representation of $J_{bo}(r)$ only in the central core of the beam. A cut-off is also consistent with the slow approach to conductivity saturation at large radii. In cases of high fractional current neutralization the growth rates do depend on the choice of cut-off, so it can be important in modeling experiments to determine the profile of $J_{bo}(r)$ or $\sigma_o(r)$ in the wings.

It is striking that the <u>scaled</u> peak growth rate τ_1 Max ω_i is nearly the same (to within ~ 30%) in all cases. But $\tau_1 \equiv \pi\sigma_o(0)\, a^2/2c$ increases rapidly with I_b; if, for example, the beam current density $J_b(0)$ on axis is held constant as I_b is varied, then the recombination saturated value of $\sigma_o(0)$ is constant while $a^2 \propto I_b$ and $\tau_1 \propto I_b$. Thus Fig. 7 shows that the actual growth rate in the beam tail Max ω_i decreases as I_b^{-1}, even though the return current fraction increases rapidly with I_b.

The strong decrease of Max ω_i with increasing I_b is due to three separate effects: (i) The conductivity channel relaxes toward the perturbed beam, thus reducing the magnetic repulsion between the plasma return current and the beam. This effect appears in Eq. (47) and thence in the f(r) term in the first factor of the right hand side of Eq. (49). (ii) The unperturbed conductivity channel $\sigma_o(r)$ is broader than the beam profile $J_{bo}(r)$, as seen in Eq. (46b). Thus much of the plasma current flows outside the beam and exerts no force on the beam. Mathematically, the destabilizing factor $[1 + f(0)]^{-1}$ on the right hand side of Eq. (49) is smaller (for $I_p/I_b < 0$) than $(1 + I_p/I_b)^{-1}$. (iii) The growth rates naturally scale inversely with the dipole diffusion time, some radial average of the quantity $\pi\sigma_o(r)a^2/2c^2$ that appears on the left hand side of Eq. (49). When $J_{bo}(r)$ and $\sigma_o(r)$ have identical Bennett profiles, the appropriate average is τ_1, defined in Eq. (4), but when the profile of $\sigma_0(r)$ is broader than that of $J_{bo}(r)$, the true dipole diffusion time $\bar{\tau}_1$ is longer than τ_1; this effect reduces Max ω_i for all cases,[2-4,17] even if $|I_p| \ll I_b$.

The numerical results of each of these effects is illustrated in Table 2. For each of the four cases calculated in Fig. 7, τ_1Max ω_i as calculated for the correct equilibrium (first column) is compared with the value obtained if the conductivity channel is not allowed to follow the beam perturbations (second column), or if, in addition, the channel shape $\sigma_o(r)$ is set equal to beam shape $J_{bo}(r)$. We note that the stabilizing effects are present in all cases, but are very strong for highly current-neutralized cases.

Table 2

Comparison of the non-dimensionalized peak growth rate τ_1 Max ω_i in the beam tail, as calculated from the correct equilibrium [$\sigma_o(r) \propto J_{bo}^{1/2}(r)$], with perturbed conductivity $\hat{\sigma}$ included, with $\hat{\sigma}$ neglected, and from a prescribed fixed conductivity channel with $\sigma_o(r) \propto J_{bo}(r)$. Four cases are considered: the first three are approximately correct values of f for a beam with the given γ injected into neutral gas, and the fourth case is for a plasma current externally constrained to be equal to I_b.

		Maximum Growth Rate τ_1 Max ω_i		
λ	f	$\sigma_o \propto J_{bo}^{1/2}$ $\hat{\sigma}$ self-consistent	$\sigma_o \propto J_{bo}^{1/2}$ $\hat{\sigma} = 0$	$\sigma_o \propto J_{bo}$ $\hat{\sigma} = 0$
0.044	-0.04	0.49	0.49	0.63
0.44	-0.3	0.53	0.58	1.20
4.4	-0.8	0.40	0.81	7.0
0.44	1	0.40	0.25	

4. Multi-Component Simulations

A. VIPER Model Description

The VIPER multi-component simulation model allows one to relax many of the simplifying assumptions of the previous sections. In particular, this code can treat the beam head region where the assumptions of constant $I_b(\zeta)$, $I_n(\zeta)$, $a(\zeta)$, and $\sigma_o(\zeta)$ are violated, and where the magnetostatic approximation to the electromagnetic fields, Eq. (5), is not valid. Because the conductivity in this region is low, considerable hose growth can occur before the beam body is reached. In addition, simulations indicate that the dominant frequency Ω observed in the beam body and tail is strongly influenced by conditions in the beam head. The sharp separation of the beam into a body and a tail, as described in the dispersion relation models, is also somewhat arbitrary since conductivity saturation due to recombination occurs first on axis and much later in the radial wings of the beam. Thus, there is a long transition region in ζ between the body and the tail.

The VIPER model treats the evolution of self-consistent fields, conductivity, and beam dynamics for both monopole (m=0) and dipole (m=1) quantities. A description of the model equations is given in the Appendix. The coordinate transformation to ζ and z discussed in the introduction is used throughout, and all quantities are radially resolved. Monopole and dipole fields are treated using the ultrarelativistic equations derived by Lee[20] for arbitrary conductivity. In addition to the beam-impact ionization term in (6), the conductivity equations include a simple E/p avalanche model and recombination. Axisymmetric beam dynamics are represented by an envelope equation which assumes that the beam expands or contracts self-similarly, maintaining a

Bennett profile. Emittance changes due to multiple scattering and anharmonic damping influence the envelope radius, as does beam energy loss due to the inductive electric field E_{zo}. Dipole beam dynamics are treated using the linearized multi-component model described in Ref. 3. Each axial segment, propagating at a fixed distance ζ from the beam head, is partitioned into several hundred components whose densities are chosen so as to reproduce the desired Bennett profile. Since the individual components have different edge radii and since each is allowed to oscillate independently in the transverse plane, the dynamics are radially resolved. The principal quantity of interest is the average hose displacement $\bar{Y}(\zeta,z)$ of these components, weighted by the individual component densities. Because the model is linearized, $\bar{Y}$ is treated as an infinitesimal (compared to the beam radius), and is normalized to the initial perturbed displacement.

B. VIPER Simulation of a 10 kA Beam

In this section, we present an example of a single VIPER simulation of a 50 MeV, 10 kA beam propagating in full density air. Parameters for the run are listed in Table 3. All distances are expressed in terms of the nominal beam radius a_o = 0.5 cm.

The beam radius a, on-axis conductivity σ_o, and "effective current fraction" $1 + f_e$ are plotted as functions of distance ζ from the beam head in Fig. 8. Here $1 + f_e$ is the pinch force, averaged over the beam profile $J_{bo}(r)$, and normalized to the value it would have if there were no plasma current and the self-fields were purely magnetostatic. Thus $f_e \approx I_p/I_b$ in the beam body, where $J_{po}(r)/J_{bo}(r)$ is approximately constant, but $1 + f_e \to 0$ in the beam head, where space charge forces largely cancel the magnetic pinch forces, and in the beam tail the difference between the profiles of $J_{po}(r)$ and $J_{bo}(r)$ is included in the definition of f_e. The beam radius $a(\zeta)$, plotted at five values of the propagation distance z/a_o between 0 and 2400, shows the processes of nose erosion[7,8] and Nordsieck expansion[21] (Fig. 8a). The conductivity $\sigma_o(\zeta, r=0)$, seen in Fig. 8b, rises linearly with ζ after I_b reaches its plateau value ($\zeta/a_o \gtrsim 50$), and until recombination saturation sets in. As a function of z, σ_o decreases slowly due to the effect of Nordsieck expansion. The effective current fraction (Fig. 8c) varies slowly with both ζ and z for $\zeta/a_o \gtrsim 50$. Thus, this beam has a substantial region where a, I_p/I_b, and $d\sigma_o/d\zeta$ are approximately constant in ζ and z, and the dispersion relation analysis for the beam body can be applied.

Figure 9 plots the average hose displacement $\bar{Y}(z)$ for ζ/a_o = 124 and 149. Because the instability is convective in the beam frame, $\bar{Y}(z)$ at a fixed location ζ initially grows, but eventually saturates and decays.

Table 3

Parameters for VIPER Simulation Example

Parameter	Symbol	Value
Maximum Beam Current	I_{bo}	10 kA
Initial relativistic factor	γ_o	100
Nominal radius	a_o	0.5 cm
Gas pressure	p	760 torr
Rise length	ζ_r	$30a_o$
Pulse length	ζ_{max}	$300a_o$
Start of perturbation	ζ_o	$20a_o$
Initial perturbation form	$Y_o(\zeta) = \sin [0.157(\zeta-\zeta_o)/a_o]$ for $20 \leq \zeta/a_o \leq 40$	
Current profile	$I_b(\zeta) = I_{bo} \tanh (\zeta/\zeta_r)$	

The frequency Ω of the hose oscillations seen in Fig. 9 varies slowly with ζ and z, so a single mode approximation in the dispersion relation (28) or (32) can be used. Taking local beam parameters at $\zeta/a_o = 149$ and $z/a_o = 600$, we have $\Omega_{\beta o}a_o = 0.057$, and $\Omega/\Omega_{\beta o} = 0.31$. Note that this value is significantly below the value $\Omega/\Omega_{\beta o} = 0.62$ expected from Eq. (32) and Table 1 for peak hose growth.

For a convective instability, the maximum ("saturated") value of $\bar{Y}$ reached at a given ζ, denoted $\bar{Y}_{sat}(\zeta)$, should increase with ζ at a power-law growth rate $\bar{\omega}_i$ in the beam body, as prescribed in Eq. (14) or at an exponential growth rate ω_i in the beam tail, as prescribed in Eq. (22). For example, $|\bar{Y}_{sat}|(\zeta)$ is 1900 for $\zeta = 124$, but is 3000 for $\zeta = 149$, as seen in Fig. 9. The plot of $\bar{Y}_{sat}(\zeta)$, Fig. 10, shows power law growth as expected. A least squares fit gives $\bar{\omega}_i^{exp} = 2.28$ for the "computer experiment" growth rate. The multicomponent dispersion relation for $1 + f = 0.57$, $\lambda = 0.44$, and $\Omega/\Omega_{\beta o} = 0.31$ gives $\bar{\omega}_i^{th} = 2.40$. (Variations if f and $\Omega/\Omega_{\beta o}$ within the beam body introduce an uncertainty of $\pm$ 0.25 in the theoretical prediction for $\bar{\omega}_i$.) The observed growth rate thus agrees well with the dispersion relation predictions for the observed value of Ω, but is substantially below the value $\bar{\omega}_i^{th} = 3.8$ predicted for the fastest growing mode, where $\Omega/\Omega_{\beta o} = 0.62$.

This reduction in hose growth rate from the theoretical maximum is seen in all VIPER simulations in which the perturbation begins in the expanded beam head. This region of the beam has a lower $\Omega_{\beta o}$ than in the body and a lower dipole decay length. Low frequency modes grow rapidly in the beam head and persist into the beam body. Higher frequency modes are stable in the beam nose and usually do not catch up with the lower frequency modes in the beam body. Thus, the observed $\Omega/\Omega_{\beta o}$ in the beam

body is substantially less than 0.62. In general, the amount of hose growth depends strongly on the extent to which Γ_{3o} varies throughout the beam.

In the example used here, the simplifying assumptions of the analytic theory of Sec. II are very well satisfied within the beam body. Even in this case, we have seen that the transition from beam head to body plays an important role in choosing the dominant value of ζ. In many other cases, the assumptions may not be well satisfied, so that the analytic theory is only qualitatively applicable. For example, the $I_b(\zeta)$ pulse shape may rise slowly or may not have a flat-top. $I_p(\zeta)$ may fall off significantly within the beam body, and therefore the beam radius may decrease as the pinch becomes stronger, particularly for high-current cases where $-1 < I_p/I_b < -\frac{1}{2}$. In such cases, code studies are essential to predict hose growth accurately. A variety of such studies, over a wide parameter range, will be presented in future reports.

5. Conclusions

We have derived dispersion relations that include conductivity evolution self-consistently (but with the important assumption of constant electron mobility) in both the equilibrium and the linearized hose perturbations of a propagating beam. We have used the dispersion relations to explore a wide range of beam and gas parameters. Particularly for cases in which there is a high degree of overall current neutralization, the hose growth rate turns out to be much less than might have been expected from previous work. We have also used the multicomponent code VIPER to demonstrate some additional effects that can modify the interpretation and use of the dispersion relations. As an example, hose growth in the beam body is usually dominated by low frequency modes that are excited at and grow rapidly near the pinch point at the front of the beam, rather than by the modes that are most unstable in the body.

Acknowledgments

The mathematical formulations presented here are new, but some of the qualitative insights have been developed over the years interactively within an interested community. In this connection, we wish particularly to acknowledge many conversations with, and access to unpublished work of Drs. Richard J. Briggs, Edward P. Lee, Simon S. Yu, and R. Leon Feinstein. We are also grateful to Dr. Steven P. Slinker for contributions to the VIPER code, and to Dr. Glenn Joyce for many contributions.

This work was supported by the Defense Advanced Research Projects Agency under ARPA Order 4395, Amendments No. 1 and 9.

Appendix

In this appendix we summarize the model equations used in the VIPER hose dynamics code discussed in Section 4. The model is based on the linearized multicomponent formulism described in Ref. 3. We represent the unperturbed beam current $J_{bo}(r)$ as a superposition of components with density profile

$$(1 - r^2/R^2)\ \Theta(R - r), \tag{A-1}$$

where

$$\Theta(R - r) \equiv \begin{cases} 1, & \text{if } R \geq r, \\ 0, & \text{if } R < r. \end{cases}$$

The edge radius R is used to index the components. Thus we can write

$$J_{bo}(r) = \int_0^\infty dR\ (1 - r^2/R^2)\ F(R)\ \Theta(R - r), \tag{A-2}$$

where F(R) is the amplitude of component R. F(R) can be calculated by differentiating Eq. (A-2) twice.[3] For a beam with Bennett profile

$$J_{bo}(r,\ \zeta,\ z) = \frac{I_b(\zeta,z)}{\pi a^2(\zeta,z)[1 + r^2/a^2(\zeta,z)]^2}, \tag{A-3}$$

we find

$$F(R) = \frac{12 I_b R^3}{\pi a^6 (1 + R^2/a^2)^4}. \tag{A-4}$$

The perturbed current $J_{b1}(r)e^{i\theta}$ is calculated by assuming that each

component undergoes a rigid linearized displacement $Y(R,\zeta,z)$ along the y-axis (perpendicular to the direction of propagation). The formal result is

$$J_{bo}(r) + J_{b1}(r)\sin\theta$$

$$= \int_0^\infty dR\ \Theta\ [R^2 - |\vec{r} - \vec{Y}(R)|^2]\left(1 - \frac{|\vec{r} - \vec{Y}(R)|^2}{R^2}\right)F(R). \qquad (A\text{-}5)$$

To take account of the fact that a slice may expand or contract, we generalize the formalism slightly by defining $\rho \equiv R/a$, and use ρ as the component index, i.e. each component expands at the same rate as a and the beam expansion is thus self-similar. Linearizing in $Y(R,\zeta,z)$ and expanding the theta function gives

$$J_{b1}(r) = \frac{2r}{a}\int_{r/a}^\infty d\rho\ \frac{F(\rho)\ Y(\rho)}{\rho^2} = \frac{24I_b r}{\pi a^4}\int_{r/a}^\infty d\rho\ \frac{\rho Y(\rho)}{(1+\rho^2)^4} \qquad (A\text{-}6)$$

for a beam of Bennett profile. In practice, the VIPER model includes only components with $\rho \leq \rho_{max} = 8$; as a result, the unperturbed current $J_{bo}(r)$, which is calculated by evaluating (A-2) for $\rho \leq \rho_{max}$, falls off more rapidly than a true Bennett distribution for $r/a \gtrsim 3$.

In VIPER we normally use a conductivity evolution equation

$$\frac{d\sigma}{d\zeta} = \kappa\ J_b + \frac{\alpha_E}{c}\sigma - \beta_r\sigma^2 \qquad (A\text{-}7)$$

which includes avalanche as well as the beam-impact ionization and recombination included in Eq. (45). (We have used more elaborate temperature-dependent conductivity models on occasion.) The avalanche

coefficient α_E is a function of the ratio of the electric field E_o to the gas density ρ_g, given as Eqs. (16) and (17) of Ref. 18. In cgs units, the recombination coefficient used in VIPER for air is[19] $\beta_r = 7.1 \times 10^{-15}(\rho_g/\rho_o)$ sec/cm, where ρ_o is the air density at standard temperature and pressure, and the impact-ionization coefficient is $\kappa = 8.6 \times 10^{-4}$cm/statamp-sec. An appropriate expansion of (A-7) gives $d\sigma_1/d\zeta$.

The electromagnetic fields are calculated using Lee's "Empulse" approximation[20] to Maxwell's equations, which is appropriate for ultrarelativistic paraxial beams. In the Lorentz gauge, these field equations are

$$\frac{c}{4\pi}\frac{1}{r}\frac{\partial}{\partial r}\, r\,\frac{\partial}{\partial r}\left(A_o^* + \phi_o\right) = -J_{bo} + \sigma_o\frac{\partial A_o^*}{\partial \zeta}, \qquad \text{(A-8)}$$

$$\frac{c}{4\pi}\frac{1}{r}\frac{\partial}{\partial r}\, r\,\frac{\partial^2 A_o^*}{\partial r\partial \zeta} = \frac{1}{r}\frac{\partial}{\partial r}\, r\sigma_o\frac{\partial \phi_o}{\partial r}, \qquad \text{(A-9)}$$

for the $m = 0$ potentials. We have defined

$$A_o^* \equiv A_{zo} - \phi_o. \qquad \text{(A-10)}$$

The corresponding $m = 1$ equations, linearized in perturbed quantities, are

$$\frac{c}{4\pi}\frac{\partial}{\partial r}\frac{1}{r}\frac{\partial}{\partial r}\, r\left(A_1^* + \phi_1\right) = -J_{b1} + \sigma_o\frac{\partial A_1^*}{\partial \zeta} + \sigma_1\frac{\partial A_o^*}{\partial \zeta}, \qquad \text{(A-11)}$$

$$\frac{c}{4\pi}\frac{\partial}{\partial r}\frac{1}{r}\frac{\partial}{\partial r}\, r\,\frac{\partial A_1^*}{\partial \zeta} = \frac{1}{r}\frac{\partial}{\partial r}\, r\left(\sigma_o\frac{\partial \phi_1}{\partial r} + \sigma_1\frac{\partial \phi_o}{\partial r}\right) - \frac{\sigma_o\phi_1}{r^2}, \qquad \text{(A-12)}$$

where

$$A_1^* \equiv A_{z1} - \phi_1. \tag{A-13}$$

Within Lee's approximation the electric field components are given by

$$E_z = -\frac{\partial A^*}{\partial z}, \tag{A-14}$$

$$\underset{\sim}{E}_\perp = -\nabla_\perp \phi, \tag{A-15}$$

and the Lorentz force on the beam electrons is given by

$$F_{Lz} = -eE_z, \tag{A-16}$$

$$\underset{\sim}{F}_{L\perp} = e\nabla_\perp A^*. \tag{A-17}$$

The boundary conditions used are perfectly conducting conditions on a cylinder at large radius, as well as the conditions that all fields vanish ahead of the beam. These field equations are valid in low conductivity regions as well as the high conductivity beam body.

Axisymmetric beam dynamics are treated using an envelope model of a type widely used in beam physics problems.[11,21] We define $\eta^2 = \bar{a}^2/a^2$, where $\bar{a}^2$ is the mean square radius of the beam (η depends weakly on the cut-off r_{max} applied to the Bennett profile[3,8]), and determine the constant η^2 by integrating $r^2 J_{bo}(r)$ out to the beam edge r_{max}. The resulting equations describing the m = 0 dynamics are:

$$\frac{d^2a}{dz^2} = \frac{\varepsilon^2 - \gamma^2 a^2 U - \gamma\, \eta^2 a^3 \frac{d\gamma}{dz}\frac{da}{dz}}{\gamma^2 a^3 \eta^2}, \tag{A-18}$$

$$\frac{d\varepsilon^2}{dz} = - \frac{2\alpha_d n a^3 \gamma^3 \varepsilon U (d^2a/dz^2)}{\varepsilon^2 + \gamma^2 a^2 U} + \bar{\varepsilon}_{sc} a^2, \qquad (A\text{-}19)$$

$$\frac{d\gamma}{dz} = \frac{e}{mc^2} E_{zo}. \qquad (A\text{-}20)$$

Here ε^2 is the squared beam emittance, U is the radially averaged pinch force, α_d is a sausage oscillation damping coefficient[22] (taken to be 0.7) E_{zo} is the axial electric field at r=0, and $\bar{\varepsilon}_{sc}$ is the multiple scattering rate,

$$\bar{\varepsilon}_{sc} = (2h\ c/e^2\ \lambda_r) \qquad (A\text{-}21)$$

where h is Planck's constant and

$$\lambda_r = 2.7 \times 10^4 (\rho_o/\rho_g) cm \qquad (A\text{-}22)$$

is the radiation length in air. The pinch force term is

$$U = - \frac{2\pi e}{\gamma I_b mc^2} \int_0^\infty dr\ r^2\ J_{bo}(r)\ \frac{dA_o^*(r)}{dr}. \qquad (A\text{-}23)$$

Finally, m=1 dynamics are described by equations for the hose displacement $Y(\rho)$ of components at a fixed value of ζ. The radially averaged y component of force on the beam component denoted by ρ is found to be

$$\frac{4\ F(\rho)\ a\Delta\rho}{(a\rho)^4} \int_0^{a\rho} dr\ r^2 \left[Y(\rho)\ \frac{dA_o^*}{dr} + A_1^* \right], \qquad (A\text{-}24)$$

where $\Delta\rho$ is the spacing between components (an infinitesimal quantity in

analytic expressions). A Newton's law equation of motion for $Y(\rho, \zeta, z)$ can be obtained by dividing out the component mass density, giving

$$\gamma \frac{\partial^2 Y}{\partial z^2} = \frac{4}{(a\rho)^4} \frac{e}{mc^2} \int_0^{a\rho} dr\, r^2 \left(A_1^* + \gamma \frac{dA_o^*}{dr}\right). \qquad \text{(A-25)}$$

A more detailed derivation of the above equations and a description of numerical methods is found in Refs. 9.

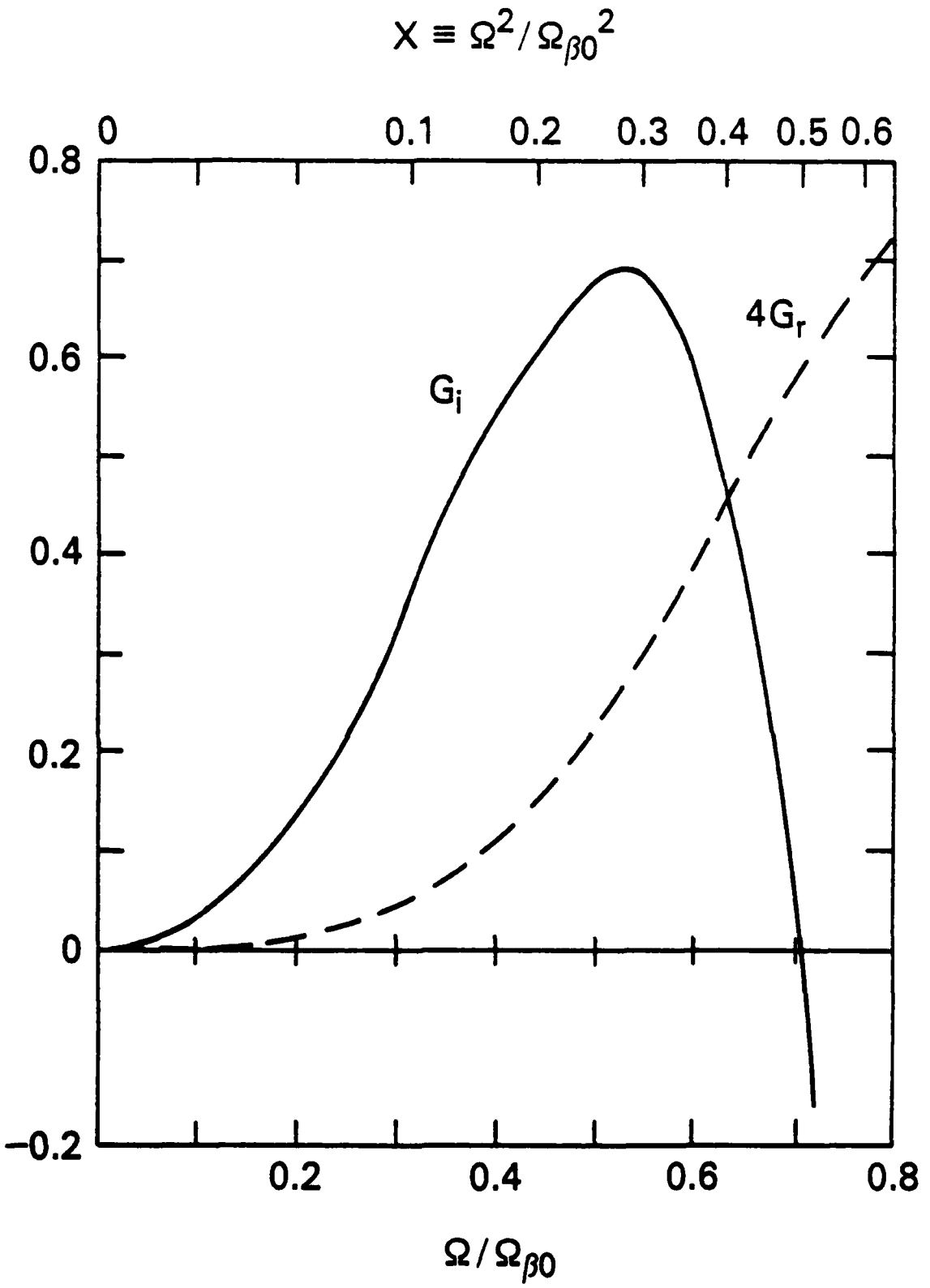

Figure 1

The complex function G defined in Eq. (26), as a function of $x \equiv \Omega^2/\Omega_{\beta o}{}^2$ (upper scale) or of $\Omega/\Omega_{\beta o}$ (lower scale).

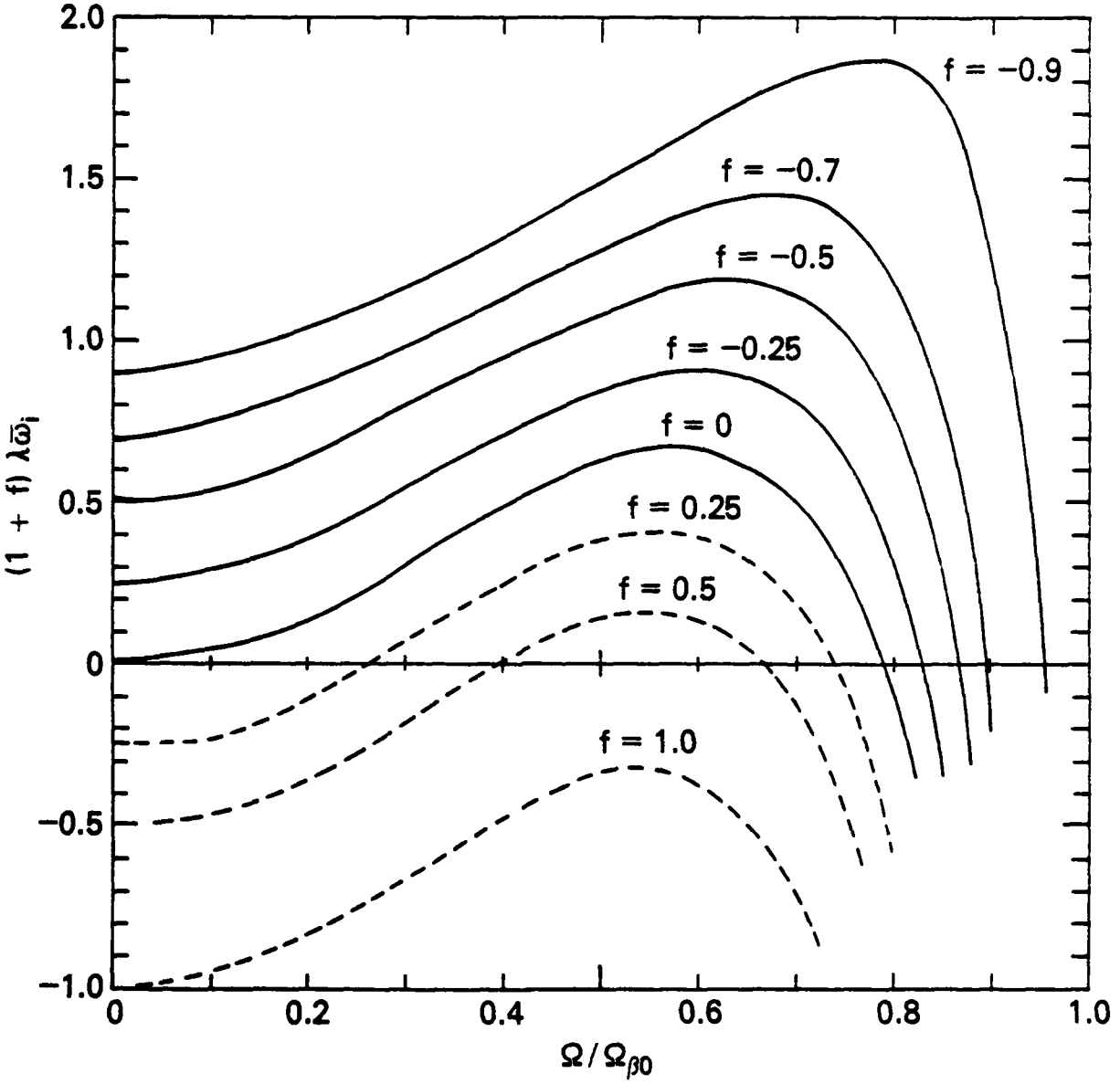

Figure 2

Growth rates in the beam body for $\lambda = 0$ and several values of f. Calculations are based on the multi-component model, Eqs. (32)-(34). Note that the ordinate is $(1 + f)\lambda\omega_i$, a form which conveniently compress the range of variation.

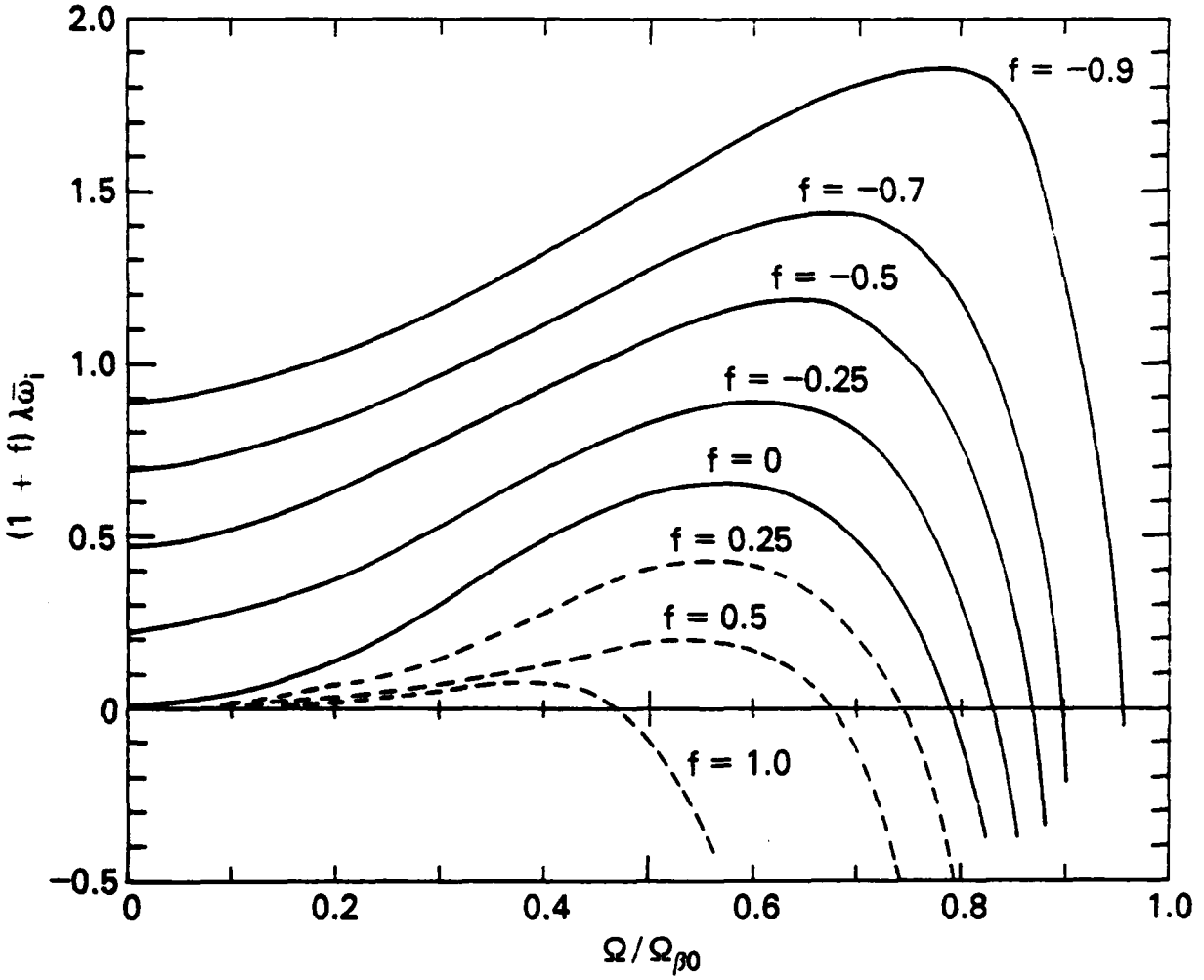

Figure 3

Growth rates in the beam body for $\lambda = 0.044$ and several values of f. Calculations are based on the multi-component model, Eqs. (32)-(34). Note that the ordinate is $(1 + f)\lambda\omega_i$.

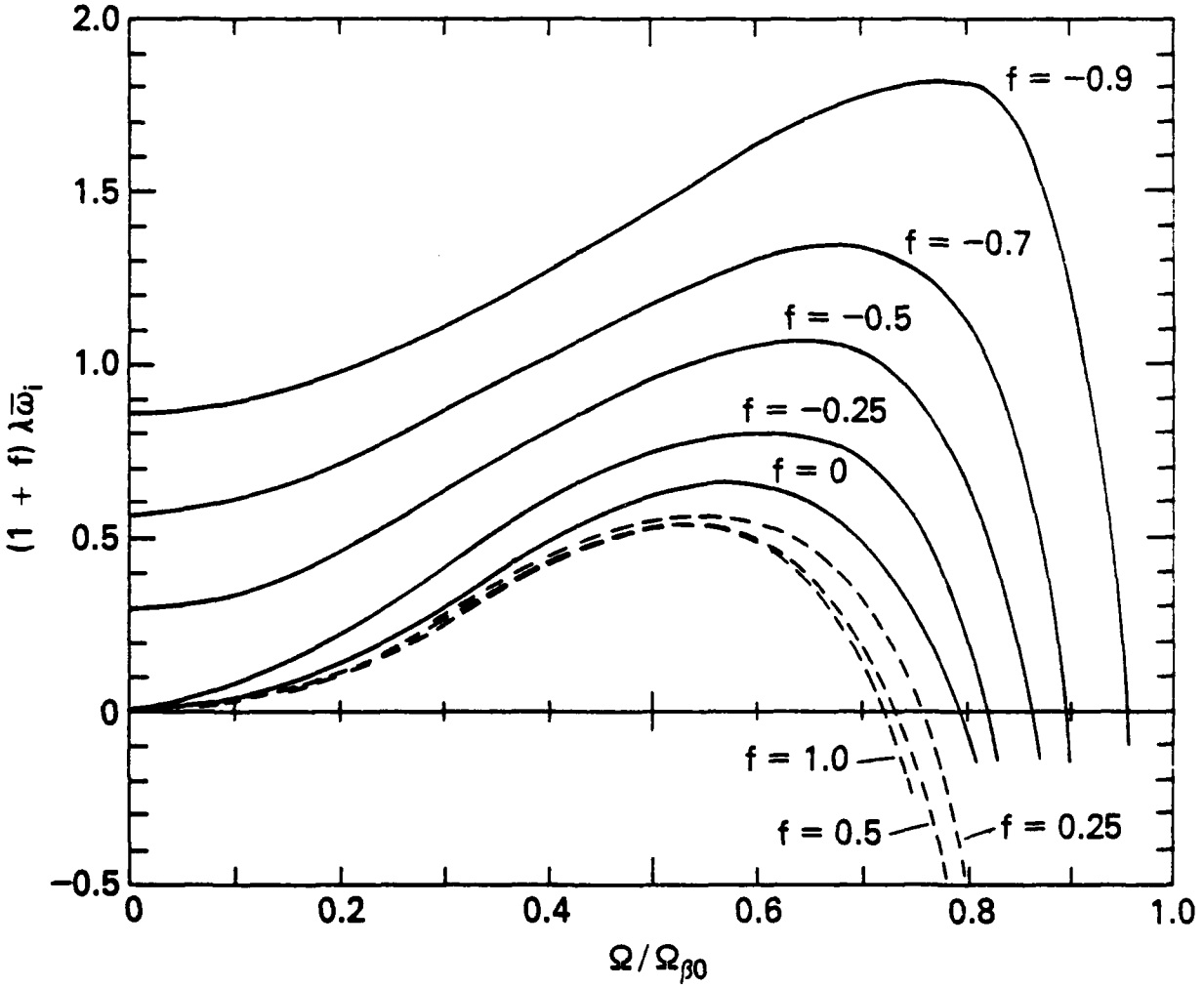

Figure 4

Growth rates in the beam body for $\lambda = 0.44$ and several values of f. Calculations are based on the multi-component model, Eqs. (32)-(34). Note that the ordinate is $(1 + f)\lambda\omega_I$.

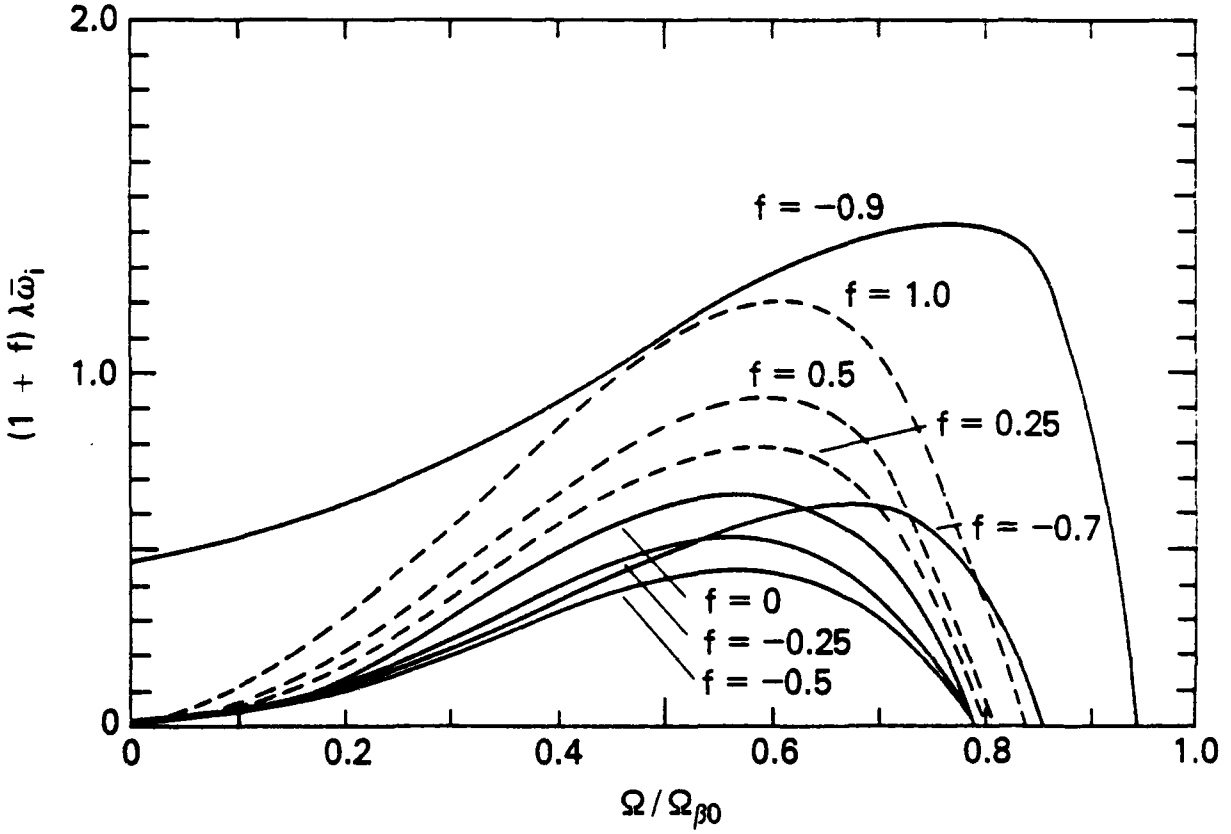

Figure 5

Growth rates in the beam body for $\lambda = 4.4$ and several values of f. Calculations are based on the multi-component model, Eqs. (32)-(34). Note that the ordinate is $(1 + f)\lambda\omega_i$.

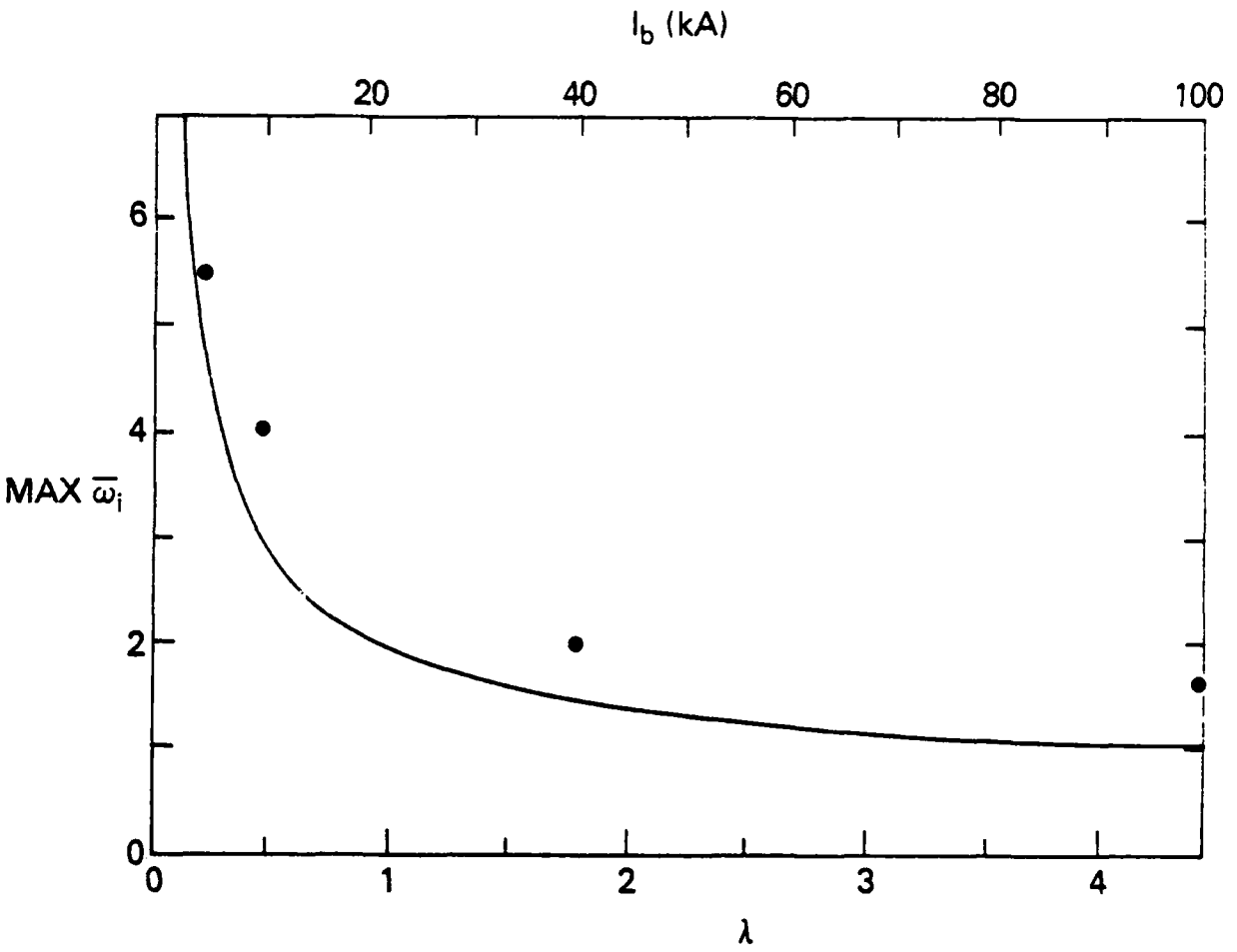

Figure 6

Maximum growth rate in the beam body, for a beam injected into neutral gas, as a function of λ (lower scale) or I_b (if the gas is air, upper scale). The curve is the theoretical result from Eqs. (42) and (43), while the dots are the results of four VIPER runs.

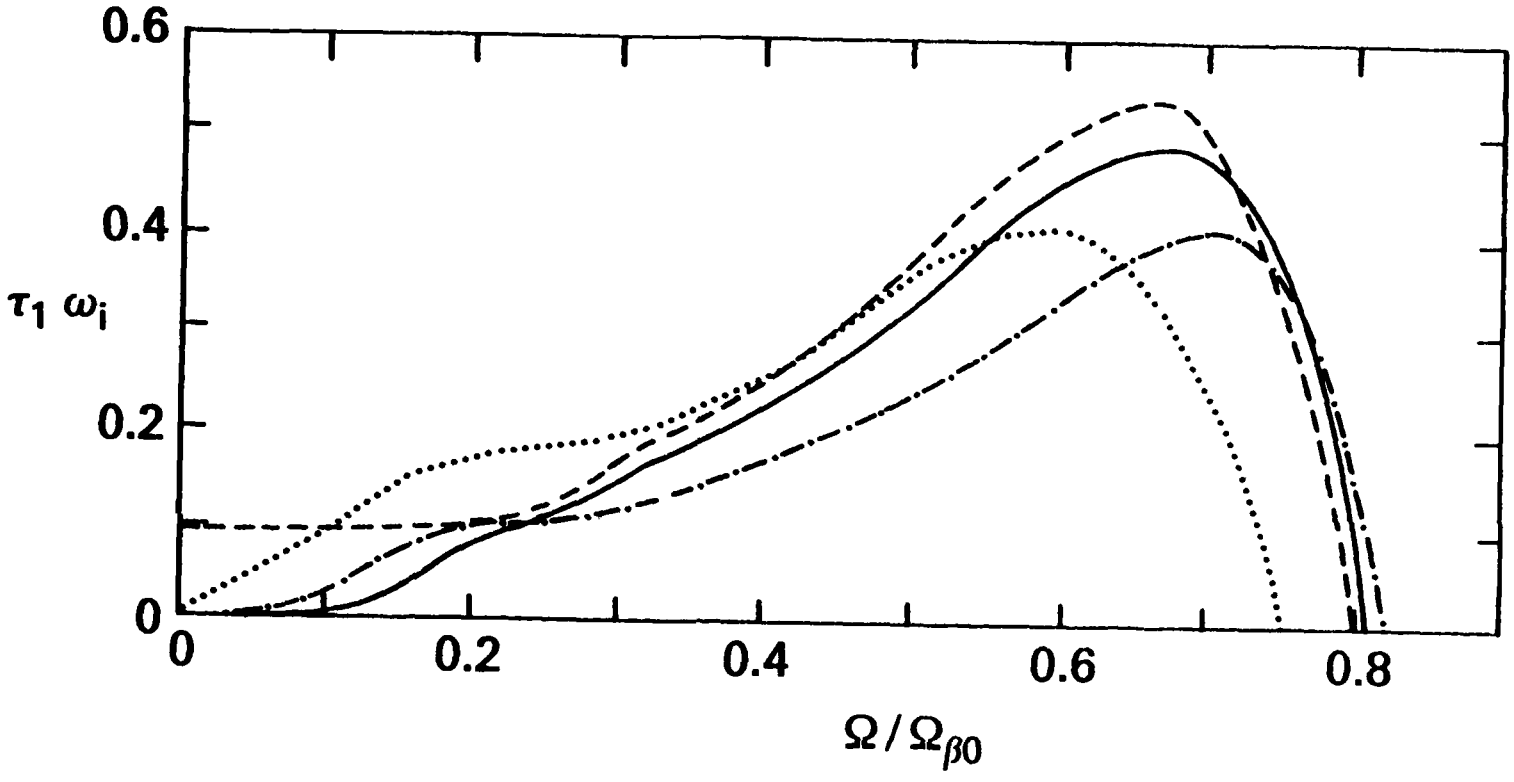

Figure 7

Growth rates in the beam tail, scaled to τ_1^{-1}, for a beam injected into neutral gas with $\lambda = 0.044$ (solid curve), $\lambda = 0.44$ (dashed curve), $\lambda = 4.4$ (dotted curve), and f given by Eq. (42). The dot-dashed curve is for $\lambda = 0.44$ and $f = 1$ ($I_p = I_b$). Calculations are based on the multicomponent model, Eq. (50).

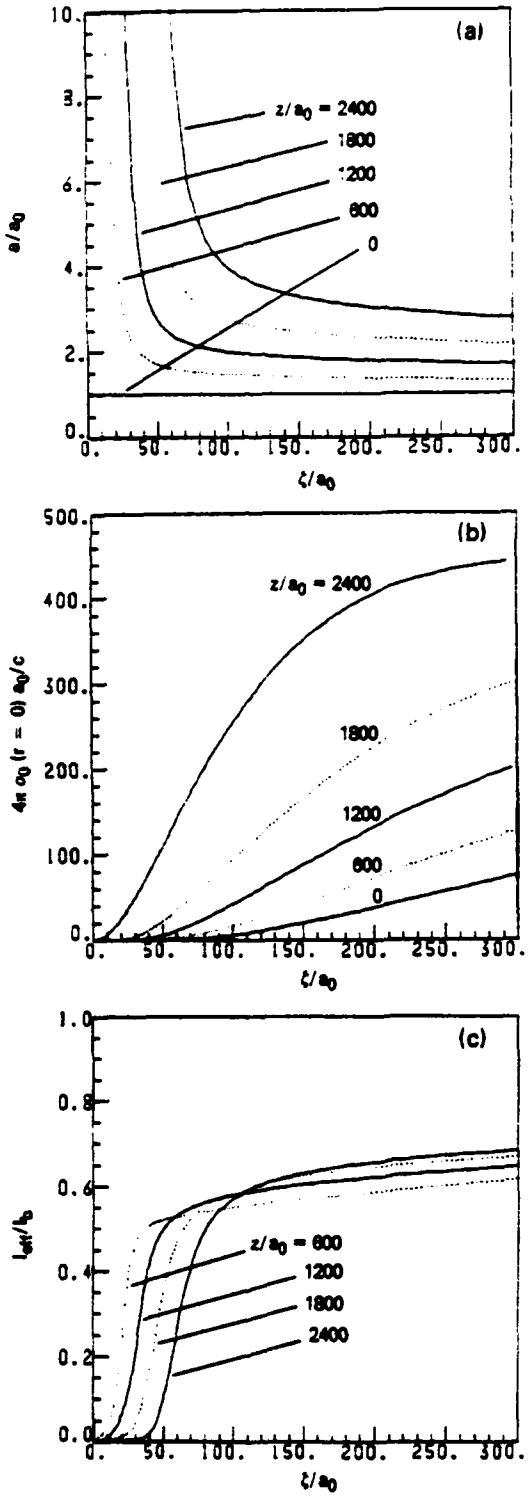

Figure 8

Beam equilibrium properties from the VIPER run described in Table 3. (a) Beam radius a/a_0, (b) conductivity $\sigma_0(r = 0)$, and (c) pinch strength $I_e/I_b \equiv 1 + f_e$, each at a sequence of different propagation ranges z.

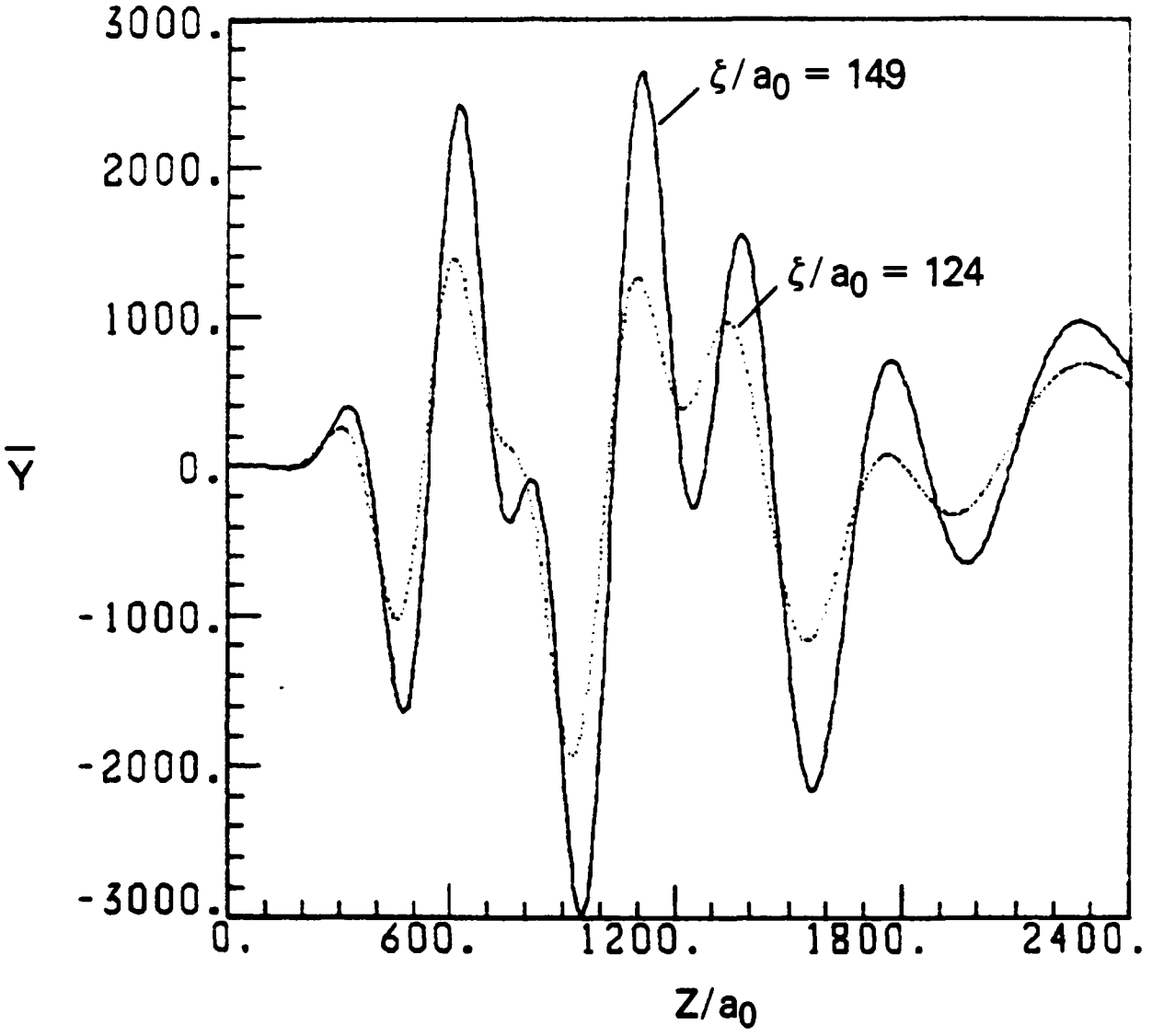

Figure 9

Hose amplitude $\bar{Y}$ as a function of z/a_o at two different locations in the beam, ζ/a_o = 124 (dotted curve) and 149 (solid curve), from the VIPER run.

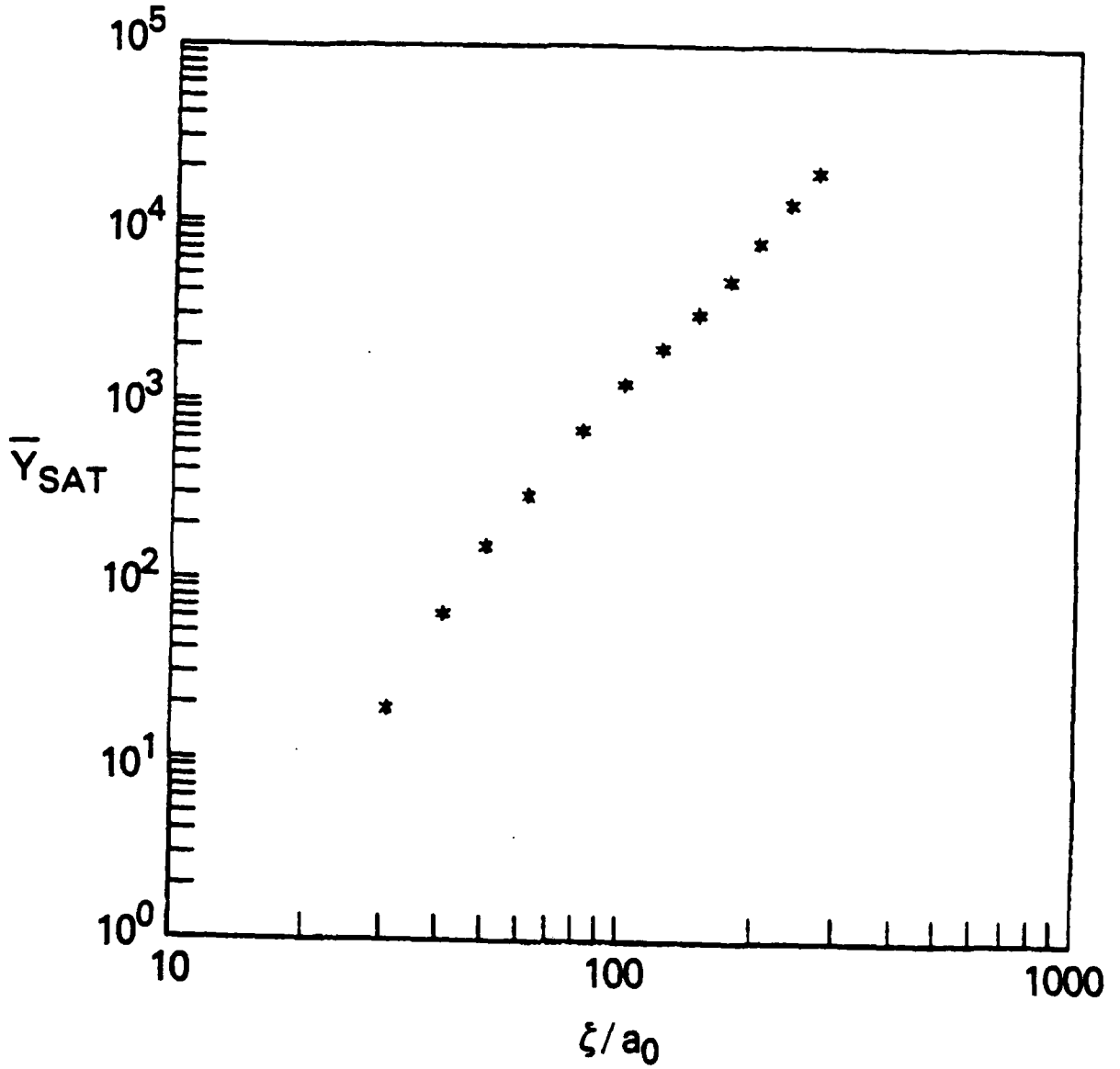

Figure 10

Saturated hose amplitude $\bar{Y}_{sat}$ as a function of ζ/a_o from the VIPER run.

References

1. E. P. Lee, Phys. Fluids 21, 1327 (1973).
2. H. S. Uhm and M. Lampe, Phys Fluids 23, 1574 (1980).
3. W. M. Sharp, M. Lampe and H. S. Uhm, Phys. Fluids 25, 1456 (1982).
4. E. P. Lee, Lawrence Livermore National Laboratory Report UCID-19639 (1982).
5. W. M. Sharp, "Vlasov Treatment of Resistive Beam Instabilities", NRL Memorandum Report, to be published.
6. R. Briggs, E. P. Lee, J. M. Leary and D. Pearlstein, unpublished.
7. E. P. Lee, "Model of Beam Head Erosion", Lawrence Livermore National Laboratory Report UCID-18768 (1980).
8. W. M. Sharp and M. Lampe, Phys. Fluids 23, 2383 (1980).
9. R. F. Hubbard, M. Lampe, S. P. Slinker, and G. Joyce, "VIPER I: A Multicomponent Hose Dynamics Code," JAYCOR Tech. Report J207-81-005(1981); "Multicomponent Simulations of the Resistive Hose Instability," JAYCOR Tech. Report J207-82-005 (1982), G. Joyce, M. Lampe, W.M. Sharp, and S.P. Slinker, Bull. Am. Phys. Soc. 26, 915 (1981).
10. G. Joyce and M. Lampe, Bull. Am. Phys. Soc. 27, 1072 (1982).
11. E. P. Lee, F. W. Chambers, L. L. Lodestro, and S. S. Yu, in Proceedings of the Second International Conference on High Power Electron and Ion Beam Research and Technology, Cornell Univ., 1977, p. 381.
12. M. Lampe and G. Joyce, Phys. Fluids (in press).

13. The particular expression (4) applies for the case of identical Bennett radial profiles for J_{bo} and σ_o. The numerical coefficient in τ_1 depends (fairly weakly) on these profiles, as discussed in Sec. III.

14. For the case $f \neq 0$, Eqs. (25) can be derived by extending the analysis of Ref. 1,or by inference from the analysis leading to Eq. (76a) of Ref. 2. Equation (29) is derived as Eq. (76a) of Ref. 2, and Eq. (25) may be inferred from the reasoning used there. The beam dynamics model used in Ref. 2 is different from the spread mass model, but leads to the same results. We note here a typographical error in Eq. (76a) of Ref. 2: the factor $(1 - f_m)^{-2}$ should be $(1 - f_m)^{-1}$.

15. The values of κ used Eqs. (37), (45) and (A7) represent an estimate roughly appropriate for air with plasma electron temperature in the range 0.5-1eV. They are based on electron-molecule momentum transfer collision rates compiled and calculated by S. Slinker and A. W. Ali in "Electron Excitation and Ionization Rate Coefficients for N2," NRL Memorandum Report 4756 (1982), based on the data of A. G. Englehardt, A. V. Phelps, and C. G. Risk, Phys. Rev. 135, A 1566 (1964); R. D. Hake and A. V. Phelps, Phys. Rev. 158, 70 (1967); and L. D. Thomas and R. K. Nesbet, Phys. Rev. A12. 1729 (1975).

16. Various generalizations of the spread mass model have been proposed by E. P. Lee, in Ref. 4, and by S. S. Yu, but it is not clear that these are directly applicable to the case where $J_{po}(r)$ is important and has a very different profile than $J_{bo}(r)$.

17. S. S. Yu, private communication.

18. G. Joyce and M. Lampe, Phys. Fluids (in press).

19. The recombination coefficient β_r used in Eq. (A-7) for air is a simple estimate based on dissociative recombination rates for N_2^+ and O_2^+ with electron temperature of the order of 1eV. The de-ionization of beam-excited air is actually quite a complex subject. NO^+ and cluster ions can increase the recomination rate somewhat, and hydrated ions can dominate if water vapor is present. Not all the recombination rates are well known. For an extended critical discussion and list of references, the reader is referred to A. W. Ali, "On Electron Beam Ionization of Air and Chemical Reactions for Disturbed Air Deionization", September 22, 1981 (AD/A104517) NRL Memo Report 4619.

20. E. P. Lee, "The New Field Equations," Lawrence Livermore National Laboratory Report UCID-17286 (1976).

21. E. P. Lee and R. K. Cooper, Particle Accel. 7, 83 (1975).

22. E. P. Lee and S. S. Yu, "Model of Emittance Growth in a Self-Pinched Beam," Lawrence Livermore National Laboratory Report UCID-18330 (1979).

END

FILMED

3-84

DTIC